CHALMERS
UNIVERSITY OF TECHNOLOGY

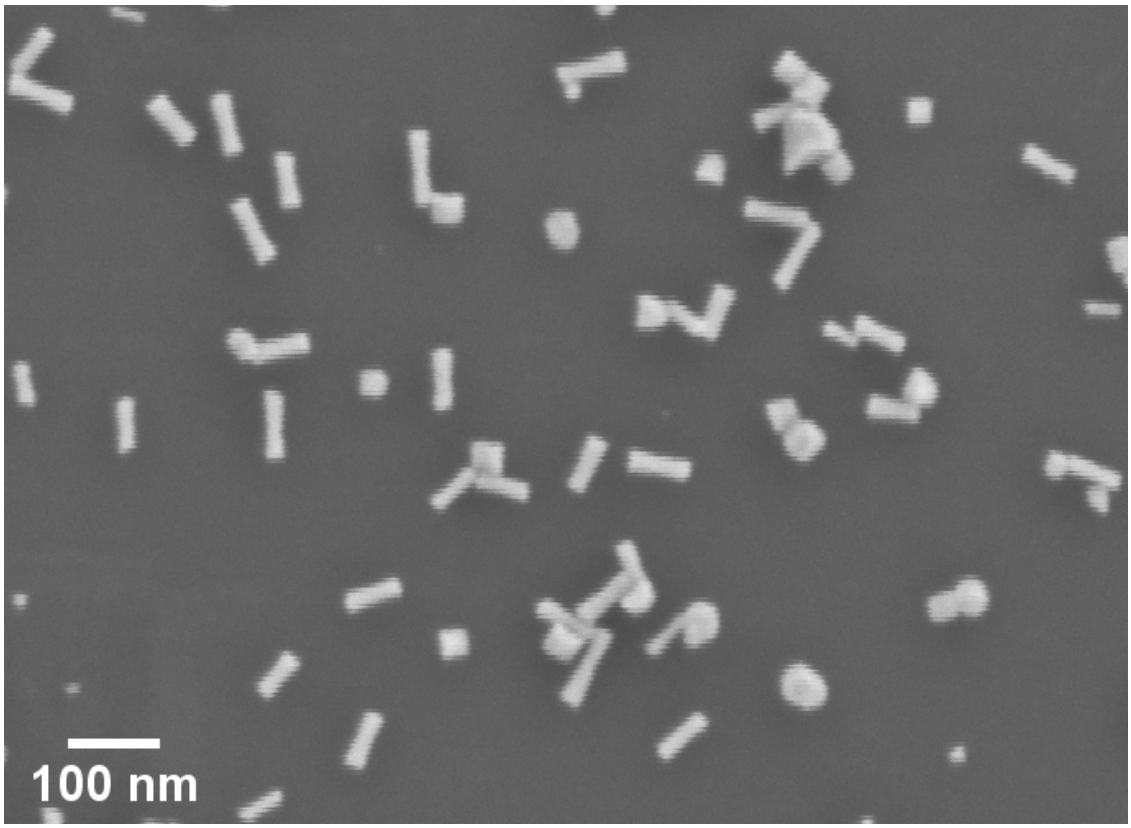

In situ synthesis of gold nanorods on SiO_2-substrates

Development of a method to grow gold nanorods directly on substrate surfaces under real-time monitoring

Master's thesis in Nanotechnology

Sean Wilson

DEPARTMENT OF CHEMISTRY AND CHEMICAL ENGINEERING
CHALMERS UNIVERSITY OF TECHNOLOGY
Gothenburg, Sweden 2023
www.chalmers.se

Master's thesis 2023

In situ synthesis of gold nanorods on SiO_2-substrates

Development of a method to grow gold nanorods directly on substrate surfaces under real-time monitoring

Sean Wilson

CHALMERS
UNIVERSITY OF TECHNOLOGY

Department of Chemistry and Chemical Engineering
Division of Applied Chemistry
M. A. Research Group
Chalmers University of Technology
Gothenburg, Sweden 2023

In situ synthesis of gold nanorods on SiO_2-substrates
Development of a method to grow gold nanorods directly on substrate surfaces under real-time monitoring
Sean Wilson

Supervisors:
Dr. Mats Hulander, Department of Chemistry and Chemical engineering
Maja Uusitalo, Department of Chemistry and Chemical engineering

Examiner:
Prof. Martin Andersson, Department of Chemistry and Chemical engineering

Master's Thesis 2023
Department of Chemistry and Chemical Engineering
Division of Applied Chemistry
M. A. Research Group
Chalmers University of Technology
SE-412 96 Gothenburg
Telephone +46 31 772 1000

Cover: SEM image of gold nanorods and a few other morphologies grown directly on a SiO_2 glass surface.

Typeset in LaTeX
Printed by Chalmers Reproservice
Gothenburg, Sweden 2023

In situ synthesis of gold nanorods on SiO_2-substrates
Development of a method to grow gold nanorods directly on substrate surfaces under real-time monitoring
SEAN WILSON
Department of Chemistry and Chemical Engineering
Chalmers University of Technology

Abstract

The implantation of a medical device introduces a high risk of infection and bacterial biofilm formation on the device surface. These biomaterials-associated infections (BAI) are difficult to treat using conventional methods, such as high dosages of antibiotic treatments, as the bacteria are protected by the biofilm. A promising treatment is to modify the implant surfaces with gold nanorods, which can photothermally eradicate bacteria beneath the biofilm with heat generated from localized surface plasmon resonance (LSPR). As such there is a need to develop methods that reliably produce gold nanorods of a size that produces LSPR at wavelengths within the biological window and that stably bind the particles to the material surface homogeneously.

In this thesis, a method has been developed to grow gold nanorods *in situ* on SiO_2-glass and silicon wafers by binding gold nanoparticle seeds to surfaces using (3-Mercaptopropyl)- trimethoxysilane (MPTMS) as a linking molecule. The seeds were then grown into rods using a modified growth solution. The method has also been adapted to surface sensitive analysis to demonstrate the increased possibility to study anisotropic nanoparticles this method brings. *In situ* quartz crystal microbalance (QCM-D) analysis was used to study the formation of the self-assembled monolayer of MPTMS, the chemisorption of gold nanoparticle seeds, and how the growth rates of the particles vary over time, possibly due to both their increasing size as well as variations in solution concentrations.

The developed method produced nanorods with a demonstrated rod yield of ~69% directly on SiO_2-glass surfaces. The rods had an aspect ratio (AR) that could be customised to tune the wavelength of LSPR. The ability to tune the optical properties of the rods could allow this method to be used to grow gold nanorods for other applications, such as sensing, as well. Here the tuning was used to demonstrate the effect of silver ions within the growth solution and to produce nanorods with LSPR at the near infrared (NIR) wavelength of ~800nm in the biological window.

Keywords: gold nanorods, localised surface plasmon resonance, NIR, biofilm, implants, photo-thermal eradication, infection, MPTMS, in-situ growth, QCM-D, in-situ analysis.

Acknowledgements

I would like to thank my examiner Prof. Martin Andersson, for providing me with the opportunity to pursue this thesis and for being so accommodating while employing me first as a student researcher. I also want to express my gratitude to my supervisors, Dr. Mats Hulander and Maja Uusitalo. All your help teaching me how to operate the instruments and answering my many questions is highly appreciated. I thank you both, as well as examiner Martin Andersson for giving such excellent guidance and support during our meetings. For always creating fruitful discussions, leading to an abundance of ideas for project directions to pursue. Your enthusiasm and encouragement has had a great impact on the project and has made each milestone all the more exciting to achieve. I would also like to thank the M. A. research group, for being supportive whenever there was any need for tips or help while dealing with lab equipment. Thank you Jenny Perez-Holmberg and Florian Schmitz for always being inclusive and engaging with the Master's students working in your lab.

This work was performed in part at the Chalmers Material Analysis Laboratory.

Sean Wilson, Gothenburg, September 2022

Contents

List of Figures

List of Tables

1
Introduction

Today, as cases of antibiotic resistance emerging in microorganisms is becoming more common, alternative treatments against infections have to be found. A common source of severe infections in patients, is the bacterial contamination on implant surfaces during surgery, vastly limiting their use. Infections of this sort are exceptionally difficult to eradicate due to the nature of bacterial reproduction while adhered to a surface, where they form a biofilm. This organic film effectively blocks out antibiotics and immune cells, requiring extended use of high dosages of antibiotics and often repeated surgeries [1][2].
The biofilms that grow on implant surfaces can reduce the effectiveness of the device and while the film grows, the infection can eventually spread further into the body of the patient. This often reaches the conclusion where the only remaining treatment option is to remove the implant, treat the infection, and then replace the device with another [2][3].

A complement, or potentially an alternative, to antibiotic treatments for biomaterials associated infections (BAI), could be to use gold nanoparticles attached to the surface underneath the biofilm. These particles can be designed to produce heat once they are irradiated with near infrared (NIR) electromagnetic radiation to photothermally eradicate the bacteria[4]. As NIR belongs to a part of the electromagnetic spectra known as the biological window, able to be transmitted through water with minimal absorption, the irradiation of the particles could potentially be done externally, through the surrounding tissue, to prevent biofilm-formation[5].
This photo-thermal coupling of gold nanoparticles is caused by non-radiative decay of localized surface plasmon resonance (LSPR), the collective oscillation of the metal's excited surface electrons, plasmons. The oscillating plasmons resonate with electromagnetic radiation, with a wavelength that depends on the particle size, generating heat during decay[6]. Anisotropic nanoparticles restricts this plasmon resonance to certain directions relative to the particle, resulting in an additional absorption band for rod shaped particles with higher absorption at longer wavelengths of light. The photothermal coupling of such particles could potentially be utilised on medical device surfaces by introducing gold nanorods and NIR, to thermally eradicate biofilm-forming bacteria that are commonly associated with implant related infections[4]. This could reduce the risk of additional surgical procedures to replace implanted devices and potentially reduce the need for extended usage of antibiotics for implant patients, an important development as the use of implanted medical devices is expected to grow with the aging population, as well as the increase in available implant treatments options[7].

Currently, anisotropic gold nanoparticles are produced mainly in two different approaches. Some lithographic methods deposit gold directly on a surface through a mask to create the desired particle shape directly on the substrate[8]. These methods require cleanroom facilities and expensive equipment however, and face difficulties in scaling up the process. Other bottom up methods rely on the chemical reduction of gold ions instead, to create a colloidal solution of nanoparticles, which later, can be purified by centrifugation to increase the rod yield and to decrease the size distribution[9][10].
The major advantages of the colloidal method, include a higher scalability of particle production and since the synthesis is performed in solution, under atmospheric conditions, the method is highly accessible and has no need of the expensive clean room facilities and equipment which are required for nanolithography. Colloidal nanoparticle synthesis still provides good control over particle sizes, shapes and distribution of both, however, care needs to be taken in regards to contamination or changes in reactant concentrations as the results are highly influenced by this[11][12].

For the use in medical implant device surfaces, the particles that are produced in solution would need to be attached in a stable way to the implant surface to avoid being released into the patients body. Such a release of particles would potentially reduce the efficacy of the treatment, as the heating effect would be lower with fewer particles and since the heating is highly local, the particles would probably need to be positioned between the surface and the biofilm for bacterial eradication. It could also leave openings on the surface devoid of any particles for bacteria to adhere to, where they would not be able to be eradicated by LSPR.

Solution-grown gold nanorods have proven difficult to attach to surfaces homogeneously using linking molecules in previous work by the research group. This has been hypothesised here to be due to difficulty for the linking molecule to reach the gold through the dense bilayer of the stabilising molecule, hexadecyltrimethylammonium bromide (CTAB), surrounding the nanorods. Growing the rods *in situ* could bypass this limitation, as the gold could then bind to the linking molecule before the particles' CTAB bilayer becomes too dense with the increased size and decreased curvature.

1.1 Purpose and objectives

In this thesis, a method has been developed to produce gold nanorods grown directly on SiO_2 surfaces using an adapted form of seed mediated growth, a colloidal particle synthesis often used when producing gold nanorods in solution. To demonstrate this, the final nanorods present on the substrate needed to be shown to have grown directly on the surface. For this the seed immobilisation needed to be verified to remain stable and that particles do not get released from the surface during the growth process. Such a release of particles would produce solution grown particles that could readsorb and invalidate results showing *in situ* growth. As such, the

seed mediated growth had to be adapted, to bind the gold nanoparticle seeds to the surface with an organosiloxane linking molecule, before being grown into larger rods.

The goal of this thesis was to develop a method of growing rod shaped gold nanoparticles directly on substrate surfaces and to demonstrate the viability of such a method for nanorod growth while achieving a high shape yield of rods, which could potentially be applied as a medical implant material surface. The gold nanorods needed to fulfill the criteria of having a tailored size and length to width aspect ratio (AR) as to allow for LSPR to occur while the particles are irradiated by electromagnetic waves within the NIR frequency range at ~800nm. This frequency range was chosen as a goal since it belongs to the so called biological window where electromagnetic radiation is transmitted through tissue[5].

Once this had been done the process needed to be optimised, allowing for reliable functionalisation of gold seeds. Then the growth solution recipe was altered to more reliably produce nanorods with a high yield, with the option to vary the shape and size of the particles to tune the LSPR band with the AR to the desired ~800nm absorbance. To verify the results and monitor the progress toward the thesis objectives, the produced solutions and substrates were analysed using ultraviolet-visible light spectroscopy (UV-vis) and scanning electron microscopy (SEM).

Another purpose of this thesis was to increase understanding of gold nanoparticle growth on surfaces and contribute to the study of the underlying growth mechanisms of anisotropic nanoparticles in general. For this purpose, the developed method has also been applied to the surface sensitive analysis technique, quarts crystal microbalance with dissipation (QCM-D), to monitor the seed immobilisation and particle growth *in situ* and in real-time.

1.2 Limitations

An ethical concern regarding this thesis work would be if there exists any toxicological implications from particles that could eventually be released from the device surfaces. This thesis however, was not able to take this into account, as it would increase the scope far beyond the set time frame, since the toxicology of larger particles is complex and need to take several aspects of the particles into account, not just the gold itself[13]. This may need to be more thoroughly examined in future studies, however, here it has been assumed that the gold particles and their adhered surfactants remain inert and harmless until flushed away during metabolic processes, as the observed cases of toxicity can mostly be attributed to left over surfactants and other reactants remaining within the nanoparticle solution[13][14].

The scope of this thesis does not include treating surface adhered bacteria with LSPR to demonstrate the photothermal eradication the rods are capable of. This has been demonstrated earlier by the research group and by others and there was not enough time left to repeat the experiment once the method developed in this

thesis to grow nanorods of the right size was completed[4][15].

Several commonplace materials used for implant devices were not investigated using the methods developed in this thesis. As this would probably have required too many parameters to be tweaked during the immobilisation and during the growth of the gold particles, for each material that is regarded. SiO_2 glass substrates were especially useful during development, as they are transparent in the visible and infrared wavelength regime. The method that was developed can however hopefully be implemented with only minor changes on such additional materials in future work, as they also commonly contain oxide surfaces.

2

Theory

2.1 Colloidal nanoparticles

A bottom up approach to make metallic nanoparticles, is the wet-chemical method of creating colloidal solutions of stabilised particles through the reduction of metal ions. The major benefit of this method is that it removes the need for expensive cleanroom equipment and facilities, with the added benefit of a high throughput of particles that can be created in a solution that can be used to functionalise several surfaces[11][12].

Maintaining a pristine crystal surface requires a larger energy of the surface atoms, as it is more energetically favourable to be a part of the bulk crystal structure, sharing their electrons with the optimal configuration of atoms. When the particles move around in the solution due to Brownian motion, this affinity for each other will cause the colliding particles to aggregate into crystalline structures, to minimise the exposed surface area and reduce the energy level of as many atoms in the crystal as possible, often assuming a spherical shape, to produce the largest bulk to surface ratio at the microscopic scale[16].

To create solutions of nanoscale particles, the particles need to be stabilised as they are created, to avoid aggregation as particles of this size will seek to minimise their surface area and if they get close enough, attractive van der Waals forces will dominate and cause aggregation[17]. Two common ways to stabilise nanoparticles in a solution as colloidal particles are either by electrostatic-, or by steric stabilisation.

Electrostatic stabilisation uses repulsive Coulombic interaction to overcome the attractive van der Waals forces, since according to DLVO theory, these interactions dominate colloidal particle behavior[17]. This is done by creating an electric double layer surrounding the particle, which is made up of a surface charge potential, a Stern layer and a diffuse layer[18]. These are created by a layer of charged surface adsorbed ions that produce the surface charge, a layer surrounding this of counterions which are closely attached electrostatically, making up the Stern layer. Finally there is a film of free ions between the Stern layer and solvent which extends out from the particle creating a diffuse layer of increased counterion concentration, which decreases radially out from the particle. This electric double layer is electrically neutral, however the electrical potential within the double layer goes from the particle's maximum, the surface charge at the surface layer, reaching outwards losing strength

exponentially with distance. The electrical potential eventually decreases to the value known as the Zeta potential, corresponding to the distance where the ionic solution is no longer attached to the particle[18]. This layer caused by the surface charge follows the particles as they drift with Brownian motion. In the colloidal solution this Coulombic Zeta potential is an important parameter, as it corresponds to the distance where inter-particle repulsion will become the particles' effective size, so collisions will slip past each other without getting close enough for van der Waals forces to cause aggregation[19].

Steric stabilisation is an entropic effect, causing a repulsive force to overcome the van der Waals interaction between particles when they get close to colliding. It works by coating the particles in longer organic molecules, forming a protective layer. Then, when the particles drift together, the organic chains will overlap, increasing the concentration of the long surface attached molecules beyond the distribution in the solution. This causes a repulsive force between the particles, as the system will tend toward a more evenly distributed state. This effect and the electrostatic repulsion from the overlapping electron orbitals will force the colloidal particles apart[20]. Some sterically stabilising molecules, for example amphiphilic molecules, form micelles around particles, dense enough to restrict masstransport to the particle inside[19].

2.1.1 Gold nanorods

Anisotropic gold nanoparticles has become widely researched, with a wide range of morphologies with varying optical and electronic properties[11][21]. These properties originate from the particles' size dependant phenomena, localised surface plasmon resonance (LSPR). The various shapes of gold nanoparticles can be grown to specific sizes, making the resulting optical properties tunable for the specific application chosen for that shape[9][11]. Such applications range from uses within electronics, sensing, surface-enhanced spectroscopy and as gold is biologically inert, they could be of use in medical device surfaces[9][11][13].

Gold nanorods in particular have highly tunable properties. The 1-dimensional anisotropy of which, removes rotational degrees of freedom of energy dissipation, reducing non radiative dampening and restricts the plasmon resonance displacement direction to either the longitudinal or the transversal direction[12]. These are some of the factors that make the longitudional absorption much larger than the spherical particle. These dimensional constraints also allow for more factors than diameter to affect the wavelength of LSPR, which become more easily adjustable over a wider range of absorption by changing the particles' length to width ratio[22].

2.1.2 Seed mediated growth

The wet chemical method seed-mediated growth is the most common method used to synthesise colloidal gold nanorods, since it produces a high yield of high quality

nanorods. The procedure is very accessible, as it does not require any specialised equipment, yet still gives good control of particle dimensions[11][12].
In this method, the key to producing a monodisperse solution of particles is the separation between the nucleation of new metallic hexadecyltrimethylammonium bromide (CTAB)-stabilised nanoparticle seeds and the growth of the 2-4nm particle seeds into larger rods. The seeds are produced by fast reduction of chloroauric acid ($HAuCl_4$) with sodium borohydride ($NaBH_4$). The surplus of CTAB molecules in the solution stabilise the particles sterically as they form, by creating a micellar bilayer surrounding the seeds[11][12].

The particles are then grown in a solution containing gold(III) and Ag^+ ions. Then, when ascorbic acid is added to the solution, the gold(III) ions in the solution get partially reduced down to Au^+ ions, since ascorbic acid's ability to reduce gold ions becomes limited at low pH. The final reduction step to metallic gold is then catalysed on the surface of the particles, limiting the reaction rate to the ionic mass transport through the CTAB stabilisation and stopping the formation of new particles. During this phase, the CTAB doubles as a shape-directing agent[12].

This method was adapted in this thesis such that instead of growing the nanorods free in a colloidal solution, the seeds have instead been attached to the surface using a linking organosilane molecule. The surface that held the seeds was then placed into a growth solution to grow the seeds directly on the surface, into appropriately sized gold nanorods. The shape and size of the particles were adjusted in this thesis by increasing the concentration of silver ions and decreasing the amount of the partially reducing agent ascorbic acid in the growth solution, which both influence the aspect ratio of the final particles[9][23].

2.1.3 Crystalline structure and growth mechanism of gold nanorods

The structural directing mechanisms driving the formation of rods is thought to be due multiple reasons. These include the preferential-binding-directed growth induced by the preferential binding of CTA^+ to the {100} face of the faceted seeds, since the atomic spacing in this plane is more similar to the CTA^+ head group. The CTAB also binds more strongly to the {110} face, since the CTAB can stabilise this facet's especially high surface energy. These effects cause a reduced crystal growth on these facets as they are blocked, breaking the symmetry of the FCC crystal structure [12][21]. The Ag^+ ions are also thought to play an important role in this structural directing by forming $AgBr-2\,(CTA^+)$ complexes, increasing the packing density of the CTAB along these facets. A significant ratio of 9% of the final rods have been found to consist of Silver[21]. Ascorbic acid may not reduce Ag^+ ions to metallic silver, but when the Ag^+ ions come into contact with facets of the metal particle, they can form a monolayer through underpotential deposition. This reduction has different rates depending on the reduction potential of the facets, suggesting that silver is deposited on the {110} side is faster than on the {100} facet, causing seeds to grow into rods[21][24]. It is also thought that the higher curvature at the tips of

the rods and around the seeds cause the CTAB interspacing to increase furter out from the particle, enabling a higher rate of ion diffusion through the CTAB layer and increasing growth in the longitudinal direction[25].

2.2 Localised surface plasmon resonance

When rough conductive surfaces, such as metals with nanoscale features, are irradiated by electromagnetic waves, the conduction electrons can be excited into collective oscillations known as plasmons, quantized units of plasma. These plasmons act as free-electron charges which propagate outward along the surface, permeating the dielectric interface between the metal and the surrounding medium[26]. The oscillation of these plasmons, will in turn resonate with incident electromagnetic waves of matching frequencies in an energy absorption phenomena called surface plasmon resonance (SPR). SPR is often used to enhance the sensitivity of surface-based optical sensing techniques, such as Raman spectroscopy, creating the new technique surface enhanced Raman spectroscopy (SERS)[27].

In metallic nanoparticles however, the conduction electrons are placed in spatial confinement, shorter than their mean free path. The wavelength of light can now be much larger than the diameter of the irradiated particle and its confined electron plasma. When such a particle is irradiated, this can result in a similar optical absorption event called localised surface plasmon resonance (LSPR). The incident electromagnetic radiation polarizes the particle, increasing its dipole moment by displacing the electron gas, which is then forced back by a restorative Coulombic interaction, causing a collective oscillation of the particle's electron plasma, through the surrounding dielectric medium. While the surface plasmons oscillate through the surrounding media, they can in turn resonate with incident electromagnetic radiation surrounding the particle, whereby the electrons absorb energy and transition to higher energy states[6][12][26].
The energy absorbed through resonance can then be dispersed through electron decay by being re-emitted as photons, widening the observed absorption peaks, and through various non-radiative transitions as heat, partially quenching the LSPR wavelength of the incident light[26].

2.2.1 Gold nanospheres

During resonance, the particle's polarization is maximised as the free electrons in the nanoparticle interact with specific frequencies of radiation. Considering this resonance frequency for a spherical gold nanoparticle, Drude's free electron model can be applied to describe the metal's electromagnetic response in terms of frequency through its dielectric function as shown in Equation 2.1[26].

$$\varepsilon(\omega) = 1 - \frac{\omega_p^2}{\omega^2 + \gamma^2} + i\frac{\omega_p^2 \gamma}{\omega(\omega^2 + \gamma^2)} \tag{2.1}$$

Here ω_p is the metal's plasma frequency, determined by the density of free electrons in the metal, γ is a damping constant, representing the various energy losses from different forms of scattering, and ω is the frequency of the incident electromagnetic field.

The resonance frequency for LSPR can then be described by analytically solving Maxwell's equations of electromagnetism at the boundary conditions surrounding the geometry of the particle surface[26]. By assuming that the field surrounding the particle is oscillatory in time, while the field strength remains constant around the particle geometry, Maxwell's equations can be solved for the polarizability of the sphere, as seen in Equation 2.2[26].

$$\alpha = 4\pi a^3 \frac{\varepsilon - \varepsilon_m}{\varepsilon + 2\varepsilon_m} \tag{2.2}$$

Where α is the sphere's polarizability, a is the radius of the sphere and ε_m is the dielectric function of the non-absorbing surrounding medium, which is proportional to the square of the medium's refractive index[28]. The resulting LSPR conditions can thus be seen to rely solely on the electromagnetic field frequency through the dielectric function[26].

The resonance wavelength for a small spherical particle can then be solved for as the field frequency which maximizes the polarization and thus the electric dipole moment of the particle in Equation 2.2, and thus the frequency for which the real part of the dielectric function fulfills the condition,

$$\varepsilon(\omega) = -2\varepsilon_m \tag{2.3}$$

The resonance frequency for a gold nanosphere can thus be seen to be determined only through the refractive index of the surrounding medium. This limits the tunability of the LSPR, as increasing the radius will only increase the extinction of visible light of approximately the same wavelength, while only changing the surrounding medium will tune the LSPR frequency[26].

2.2.2 Gold nanorods

The anisotropy of gold nanorods creates a symmetry-breaking dimensional confinement on the polarizability of the particles. This anisotropy creates additional resonances, as two dimensional axes are equal transversally with rotational symmetry across the rod, with degenerate vibrational modes, which no longer apply along the third axis. A new resonance vibrational mode appears along this separate unique axis following the length of the rod[11].

The LSPR conditions for gold nanorods can be approximated by applying the Quazistatic solution to Maxwell's equations described in subsection 2.2.1 to Gans's solution for the vibrational resonance modes in a prolate spheroid [11][26][29].

The polarizability for all axes of such a gold ellipsoid is given by,

$$\alpha_{x,y,z} = V \frac{\varepsilon(\omega) - \varepsilon_m}{\varepsilon_m + L_{x,y,z}(\varepsilon(\omega) - \varepsilon_m)} \tag{2.4}$$

Where V is the volume of the ellipsoid and $\varepsilon(\omega)$ is the wavelength-dependent dielectric function of gold. $L_{x,y,z}$ is a depolarization factor arising from the anisotropy, describing the dependence of LSPR on the particle's aspect ratio (AR). The depolarization factor is decribed below in the longitudional mode, or x dimension. The sum of the depolarization for each axis is equal to 1, giving the transversal mode, or y and z dimensions.

$$\begin{aligned} L_x &= \frac{1-e^2}{e^2}\left(-1 + \frac{1}{2e}\ln\frac{1+e}{1-e}\right); \\ L_{y,z} &= \frac{1-L_x}{2} \end{aligned} \tag{2.5}$$

e is the eccentricity of the ellipsoid described by the relation between the radius of the long axis r_x and the radius of the short axis $r_{y,z}$, similar to the AR of a rod.

$$e = \sqrt{1 - \frac{r_{y,z}}{r_x}} \tag{2.6}$$

To maximise the polarization presented in Equation 2.4, resonance occurs as the denominator is set to zero. Solving then for the longitudinal depolarization factor, L_x, during resonance gives the relation between ellipsoid eccentricity, or AR in rods, and the dielectric functions of gold and the surrounding medium.

$$L_x = -\frac{\varepsilon_m}{\varepsilon(\omega) + \varepsilon_m} \tag{2.7}$$

This demonstrates the possibility to tune the wavelength of LSPR for gold nanorods by varying the AR in relation to the surrounding medium. ε_m is a constant property of the dielectric solvent, while $\varepsilon(\omega)$ of gold is affected by the frequency of the incident electromagnetic field according to Equation 2.1.

The effect of LSPR can be observed in gold nanorods by the absorption of the specific resonance wavelengths. As seen, these resonance wavelengths vary based on the choice of surrounding medium and the dimensions of the particles. By using Ultraviolet-Visible light (UV-vis) spectroscopy, the absorption of these resonance wavelengths can be detected. A characteristic UV-vis plot for a solution containing purified gold nanorods can be seen in Figure 2.1.

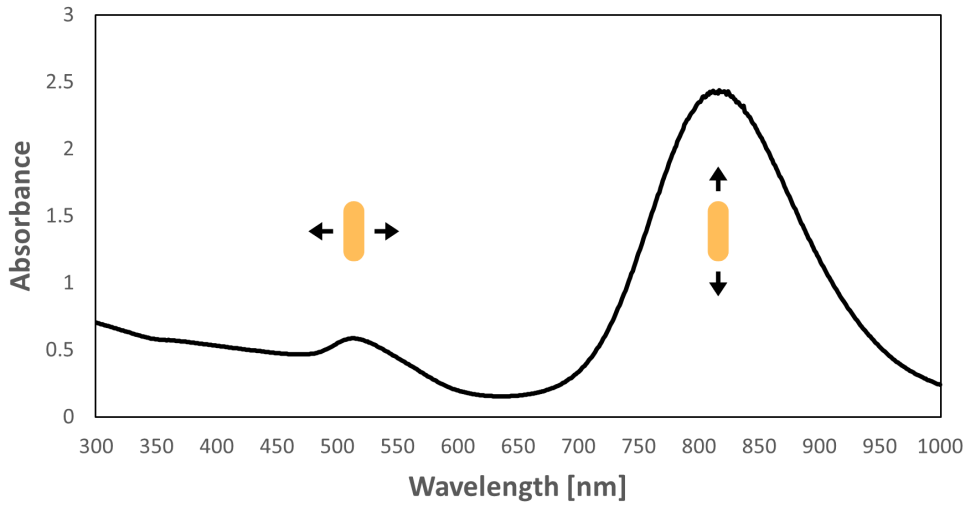

Figure 2.1: A graph showing the UV-vis absorption spectra of a solution of purified gold nanorods in water, produced from previous work by the research group. The nanorods had an aspect ratio of ~3.3 with an average length and width of 69x21nm

The larger absorption peak at ~820nm represents the longitudinal LSPR and the lower absorbance at ~520nm represents the transversal LSPR[12].

2.3 Assembly of gold seeds on substrate surfaces

Nanoparticles that are produced in solution need to be attached in a stable way to the implant surface. This can be done using linking molecules, such as organosilanes, which contain both organic and inorganic functional groups. In this thesis a thiolated organosilane, (3-Mercaptopropyl)-trimethoxysilane (MPTMS), was used to chemisorb the particle to the surface. This molecule is suitable, since it contains a thiol group (-SH) on one end, which form a gold-sulphur bond to hold onto the particle, as well as a silane group ($Si(OCH_3)_3$ at the other end, which can readily hydrolyse to bond with the silica surface or other silane groups[30].

2.3.1 Substrate preparation and self assembled monolayer formation

To create a homogeneous and dense layer of gold nanoparticle seeds, that remains stable in the presence of ions, it is desired to chemisorb the seeds to a self assembled monolayer (SAM) of the linking molecule MPTMS on the silica surface. This monolayer is formed according to the steps outlined in the schematic presented in Figure 2.2.

This method and molecule is useful when working with silicate or metal oxide surfaces. In this thesis silicon wafers and silica glass substrates were used for the synthesis. Silicon wafers was used for its atomically plane surface to optimise conditions for SAM-formation, while the silica glass substrates were favoured during

later stages while optimising the particle growth, due to its applicability in UV-vis measurements.

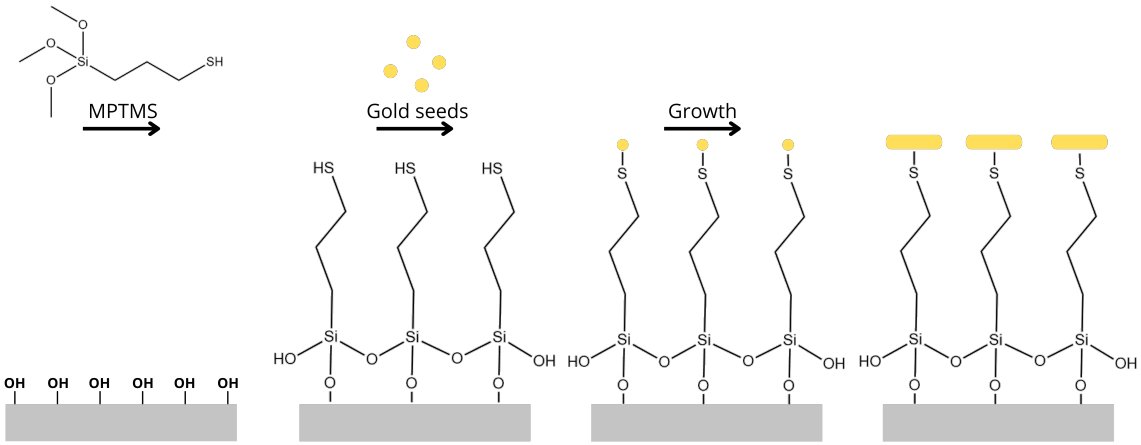

Figure 2.2: A schematic illustration depicting the steps for direct formation of gold nanorods on a SiO_2-glass or silicon wafer substrate

The steps seen in Figure 2.2 are as follows. First the pristine silicate substrate is placed in a solution of ethanol and MPTMS, where residual water adsorbed on the substrate hydrolyse and activate the MPTMS, allowing the molecules to bind into the surface and each other. The substrate is then placed in the aqueous gold seed solution, where seeds will chemisorb to the substrate by forming gold-thiol bonds with the thiol end of the MPTMS, before subsequently being placed in the growth solution, to grow into rods. Care is taken during the first step to avoid any addition of excess water into the MPTMS/ethanol solution, as this could cause polymerisation of MPTMS[30].
The silica substrates need to be free from any organic contaminants and maintain a chemically pristine surface for the SAM to form properly. This is done by excessive cleaning steps detailed in subsection 3.2.2, including an overnight bath in nitric acid (65%), to etch away any contaminants bound to the surface before synthesis.

2.4 Analytical methods

The various analytical methods that were utilised to analyse the samples and to monitor the progress of the project, along with the way they were used is presented in this section.

2.4.1 UV - Vis spectroscopy

Ultraviolet- Visible light (UV-vis) spectroscopy functions by emitting electromagnetic waves with wavelegths making up the specrum between ultraviolet and near-infrared, which is transmitted through the sample, to the detector. The light absorbance of the sample is then shown as the difference between the intensity of the detected- and the emitted light for each wavelength, as seen in Equation 2.8

$$A = -\log(I/I_0) \tag{2.8}$$

where A is the absorbance, I is the detected intensity and I_0 is the intensity of the emitted light.
LSPR occurs while gold nanorods are irradiated, as described in section 2.2, which can be seen as absorptions of specific wavelengths of light, corresponding to the electron plasma displacement across the particle. For gold nanorods, this can be seen as two peaks in the UV-vis spectrum, one arising from the transversal direction of the rod and one for the longitudional direction, giving an indication of the AR of the particle. A higher absorbance in the peaks indicates a higher density of particles at the surface.

This method utilised as the main analysis method, due to its availability and its fast results. It was used to monitor the growth process by transmitting the light through glass substrates that were functionalised with gold nanoparticles to give an indication of the shape, size and surface coverage of the particles. The method was also utilised to analyse the growth solution after the synthesis, to verify that the gold seed functionalisation of the surfaces was successful and remained stable during growth. UV-Vis was also applied to study the growth of the particles *in situ*.

2.4.2 Scanning electron microscopy

In scanning electron microscopy (SEM), data such as topology and chemical composition can be determined by raster scanning the sample with an electron beam. The electron microscope used for analysis in this thesis, SEM-Ultra, fires electrons with an electron gun by thermionic emission, where a filament heats the anode to release electrons. These electrons are then accelerated in an electric field and are focused and directed through magnetic fields and exits the electron cannon through an aperture, the size of which can be adjusted. Increasing the numerical aperture increases the resolution limit of the microscope by limiting spherical aberration[31]. Equation 2.9 shows the general relationship between maximum resolution and numerical aperture.

$$d = \frac{\lambda}{2} NA \tag{2.9}$$

Where d is the maximum resolution, λ is the wavelength of the electrons, and NA is the numerical aperture.

When the incident electron beam reaches the substrate surface, the beam of electrons can either be scattered by the electrons within the sample, excite the electrons in the sample to induce stimulated emission of high energy photons such as X-rays, or knock outer shell sample electrons out of their orbitals through inelastic interactions, releasing secondary electrons[31]. Each of these effects can be measured through the various detectors in the SEM, which can be used to either produce a

topological image or to analyse the chemical composition of the sample, by correlating the detection with the location of the raster scan.

2.4.3 Quartz crystal microbalance

Quartz crystal microbalance with dissipation (QCM-D) can be used to measure changes in the mass and rigidity of a surface on the nanoscale. Quartz crystals have an acentric crystal structure, causing them to be piezoelectric, meaning that an electrical current can be achieved through the deformation of the crystal lattice in a specific dimension. Conversely, when an alternating electrical current (AC) is applied to a quartz crystal, the crystal lattice will be deformed and begin to oscillate at the crystal's resonance frequency. This resonance frequency and its harmonic overtones are inversely proportional to the thickness of the crystal, with the commonly used quartz substrate resonance frequency of 5MHz, corresponding to a crystal thickness of approximately $330\mu m$[32].

By measuring the shift in resonance frequency during the experiment, the change in mass of the substrate over time can be determined.

$$\Delta m = -C\frac{\Delta f}{n} \tag{2.10}$$

where,

$$C = 17.7\frac{ng}{cm^2 Hz}$$

The change in frequency is denoted as Δf, $C = 17.7$ is the Sauerbrey constant for a 5MHz quartz crystal, Δm is the corresponding change in mass on the substrate and n is the harmonic mode number, also known as overtone. The energy dissipation D of the oscillations is also measured by pausing the current while measuring the dissipating voltage per oscillation. This can be used to study the viscoelasticity of the surface layer. This can give an indication during the experiment if the material adsorbing to the substrate is crystalline or amorphous and whether it extends further out from the substrate surface, as a softer material which reaches further into the solution would dampen the oscillations more quickly[32].
In this thesis, QSX 303 SiO_2 sensors from Biolin were used as substrates to study the growth rate of gold nanoparticles in real-time, as these have a sputtered 50nm layer of silica glass on the quartz crystal, which would better mimic the surface chemistry of the substrates used outside of the QCM-D experiments. The pristine surface roughness of the substrates remains low ($>$ 1nm) after this sputtering treatment.

3
Methods

In the following sections the experimental work is presented, describing the method developed in this thesis to growth gold nanorods directly on substrate surfaces. First the materials used for the thesis is presented, followed by the experimental procedure to grow gold nanorods directly on SiO_2-surfaces, and finally how the substrates were analysed, including the adaptations to the experimental procedure for *in situ* analysis.

3.1 Materials

3.1.1 Chemicals

The chemicals used during the experimental part of the project can be seen in Table 3.1, when diluted chemicals are used, the new concentration will be referenced in the text. All water that was used for diluting chemicals or for experimental purposes was purified Milli-Q Academic water, treated through a water purification system from Millipore.

Table 3.1: List containing a description of the chemicals used in this thesis, along with the suppliers they were purchased from

Name	Supplier	Description
Ammonia	Merck	32%
L-Ascorbic acid	Sigma-Aldrich	$C_6H_8O_6$ 99%
CTAB	Sigma-Aldrich	hexadecyltrimethylammonium bromide $\geq$ 99%
Ethanol	Solveco	C_2H_5OH 99.5% analytical grade
Ethanol	Solveco	C_2H_5OH 95% analytical grade
Gold(III) chloride trihydrate	Sigma-Aldrich	$HAuCl_4 > 99.9\%$
H_2O_2	Fisher	Hydrogen peroxide > 30%
Hydrochloric acid	Sigma-Aldrich	$HCl \geq 37\%$
MPTMS	Sigma-Aldrich	(3-Mercaptopropyl)-trimethoxysilane 95%
Nitric acid	Sigma-Aldrich	HNO_3 65 – 67%
Silver nitrate	Sigma-Aldrich	$AgNO_3 > 99.9\%$
Sodium borohydride	Sigma-Aldrich	$NaBH_4$, > 99% ReagentPlus®
Sodium dodecyl sulfate	Sigma-Aldrich	SDS > 99.9%

3.2 Experimental

3.2.1 Seed mediated growth

The gold seeds were synthesised by the method proposed by L. Scarabelli *et al.*[9]. In this method, CTAB stabilised gold nanoparticle seeds are produced at $30°C$ by the fast reduction of gold(III) chloride trihydrate through the addition of sodium borohydride.

First $4.7ml$ CTAB ($0.1M$) was heated to $30°C$ to dissolve the CTAB in the water. Then 25μl $HAuCl_4$ ($50mM$) was added and the solution was stirred at $400RPM$ for 5 minutes to mix thoroughly, after which 300μl $NaBH_4$ ($10mM$) was added quickly while stirring at $1400RPM$. When the solution rapidly shifts to a brown colour, the $HAuCl_4$ has been reduced to small ($2-4nm$) metallic gold nanoparticle seeds.

To minimize the size distribution of the nanoparticles, the sodium borohydride was freshly mixed and heated to the same temperature as the solution before mixing. It was then added quickly at a very high rate of stirring to optimise for quick mixing within the solution, to make sure the reduction to metallic gold occurs simultaneously, at the same rate, everywhere in a homogeneous solution.

To minimise the chance of particle aggregation or Ostwald ripening, the seed solution was attached to the surface functionalisation directly after being synthesised.

3.2.2 Gold seed functionalisation

The gold nanoparticle seeds were attached to glass surfaces and to silicon wafers with MPTMS, using the following method.
Glass microscopy slides were first cut into 1 by 1 cm pieces and the silicon wafers were ordered pre-cut into 8 by 8 mm pieces. The glass substrates were then cleaned by ultrasonication using a cleaning bath model USC900D from VWR at intensity level 9, in ethanol (99.5%) for 20 minutes and were then thoroughly rinsed in water, after which they were placed into a nitric acid bath overnight, for 15 hours. The silicon wafers were cleaned additionally before being placed in nitric acid, to remove any traces of adhesives from the cutting process, by adding a 20 minute bath in a basic piranha solution, containing a 4:1:1 ratio of water:ammonia:H_2O_2, after the ultrasonication step. They were then submerged instantly in water, which was diluted until no trace of nitric acid remains. Then the water was diluted until it was completely exchanged with ethanol (99.5%) in preparation for the functionalization.

The clean substrates were then submerged in a solution containing $10ml$ ethanol (99.5%) and 1μl MPTMS (95%) for 30 minutes to functionalize with MPTMS. Once finished, the solvent was diluted until it was completely exchanged, first with ethanol and then with water. This was done in two steps to avoid polymerisation of any remaining dissolved MPTMS molecules in the presence of water. The substrates were then transferred to the gold seed nanoparticle solution for 20 minutes to attach

the seeds to the substrates by bonding to the thiol end of the MPTMS.

3.2.3 Nanorod growth

The gold seed-functionalised substrates were then placed in a growth solution, to grow the seeds into gold nanorods. The concentration of some reagents in the solution were varied to adjust for the changed conditions of growing into rods while being attached to a negatively charged surface.

The growth solution was made by first heating 10ml CTAB ($0.1M$) to $30°C$ to dissolve the CTAB in water. Then 190μl hydrochloric acid ($1M$) and 100μl $HAuCl_4$ ($50mM$) was added and the solution was gently shaken, to mix while minimizing the generation of foam. Then, 120μl silver nitride of varying concentrations ($10mM$, $11mM$, $12mM$, 13, $14mM$, or $20mM$) was added. After shaking gently for 5 minutes to mix thoroughly, 100μl ascorbic acid of varied concentrations ($100mM$, $90mM$, $80mM$, or $70mM$) was finally added to the solution. The growth solution was then stirred vigorously until it turned colourless, indicating the reduction of gold(III) to gold$^{(1+)}$ ions[9].

Gold seed-functionalized substrates were then added to individual wells containing 1.5ml growth solution each. The seeds were then allowed to grow for 2 hours, while the temperature was kept at $30°C$ within the wells. When the growth was finished, the solution was exchanged to water, and then to ethanol (99.5%), before drying with nitrogen gas. The substrates were then stored in individual wells, covered by a lid, for later analysis.

3.3 Analysis

3.3.1 UV-Vis

The UV-vis models used in this project was a Thermo Scientific NanoDrop™ One/ OneC Microvolume UV-Vis Spectrophotometer and a Hewlett Packard 8453 Spectrophotometer. The NanoDrop™ was used for quick analysis of a few microlitres of the growth solution during and after synthesis, while the Hewlett Packard 8453 was used for analysing the prepared glass substrates and also to analyse the growth occurring *in situ* on the substrate surface in separate experiments. The base-line was set to either unused growth solution, to check for particles that had been released from the surface, or water, to determine the size-dependent absorbance in a dielectric environment similar to the human body.

In preparation for UV-Vis analysis, the finished substrates were placed in a standing position in water-filled cuvets with a path length of 10mm. The cuvets were then positioned in the instrument such that the glass substrate would cover the largest possible area of the beam of light.

The Hewlett Packard 8453 Spectrophotometer's sample mount was fitted with internal tubing, that could be connected to a heat pump, allowing for the possibility of analysing the growth process *in situ*, to compare with the results gained from QCM-D. To perform this analysis, 10x25mm glass samples were first prepared according to subsection 3.2.2, while the heat pump was set to $30°C$. The substrates were then transferred to 10mm cuvets filled with growth solution, which were placed in the heated sample mount, along with a cuvet containing non-functionalised glass and growth solution to set the baseline. During the particle growth, UV-vis measurements were performed continuously, with each sample being analysed every 5 minutes over a 2 hour period. A larger substrate size was used during this experiment to consistently be able cover the path of the light travelling to the detector.

3.3.2 SEM

Scanning electron microscopy (SEM) was used to construct images of the grown particles on the surfaces and to determine the size dispersion, coverage, shape and size of the gold nanoparticles. The SEM model LEO Ultra 55 from Zeiss was used for visualising the gold nanoparticles by detecting secondary electrons with either the inlens sensor or the SE2 detector inside the sample chamber. The images produced through the exposure were subsequently analysed using the open-source software ImageJ. By setting a threshold for the grey scale pixels, a binary image was created where the nanoparticles appeared as white pixels and the rest of the image was removed. After setting the distance scale to match the data from the SEM, the software was then used to count neighbouring white pixels compared to black pixels to decide the surface coverage of particles. ImageJ was also analysed the dimensions and circularity of the connected white pixels, which were used to filter for rod-shaped particles and gain the AR of the particles in the image. By manually removing a line of pixels between neighbouring particles, the thresholded image could be used to count the number of particles more accurately and the number of rods could be compared to the total number of particles to gain the rod yield.

The glass and wafer samples were mounted on SEM stubs with conductive carbon adhesive tape, which were subsequently mounted onto the stub holder that could be mounted in the Ultra 55 SEM. The QCM-D substrates were fastened to an S-clip sample holder, which was mounted in the SEM. The glass and Si substrates were then analysed using secondary electron detection with an acceleration voltage of 2kV at a working distance of ~7mm and 5kV at ~4mm respectively, sometimes using the inlens detector for the wafer-grown particles.

3.3.3 QCM-D

The instrument QCM-D E4 from Biolin Scientific was used to monitor the particle growth, *in situ*, on functionalised substrates, as well as during the full experimental process as described post-cleaning. The nanoparticle growth was done both with and without flow of growth solution through the modules, to study the effect. All solutions that were pumped were kept at the same temperature of $30°C$ to promote

mixing and reduce formation of bubbles in the tubes. QSX 303 SiO_2 sensors from Biolin were used as substrates, to ensure similar surface chemistry to the glass and silica substrates from the other experiments.

The surfaces were cleaned according to the protocol suggested by Biolin, for thorough cleaning. First they were UV/ozone treated for 10 minutes, then they were immersed in a solution of 2% sodium dodecyl sulfate (SDS) in water for 30 minutes. They were then kept wet until they could be thoroughly rinsed with water, to avoid surfactant adsorption. They were then dried with N_2-gas, before finally being treated with UV-ozone cleaning for 10 minutes.

To monitor the particle growth, the sensors were first cleaned additionally after the suggested cleaning by Biolin and functionalised with gold nanoparticle seeds. This was done using the same method used outside of the QCM-D, as described in subsection 3.2.2, to remain as similar to the developed method outside the QCM-D as possible, with the exception that the ultrasonication was performed at intensity level 2 to avoid any damage to the gold contacts. The substrates were then placed into Qsense flow modules, which were pumped through with water immediately, to keep the surfaces wet. The flow was set for the whole experiment to 25μl/min for each module, a value chosen based on the total volume of growth solution available. After calibrating the QCM-D E4 to the modified substrates, the measurment was started. The frequency change was then examined before moving forward, as to remain stable without drifting while submerged in the flow of water, which was repeated between each step. Then a solution of CTAB (0.1M) was pumped through the module as a baseline with a viscosity more similar to the growth solution. After this the growth solution were pumped through the modules, which was subsequently stopped for 2 of the 4 flow cells, once the solution within the chambers had been exchanged. The growth continued for 2 hours before changing back to the baseline CTAB solution. Once stable it was pumped with water, flushing away excess surfactants and reagents. The measurements were then stopped and the substrates were dried with N_2 before being stored for SEM.

For the full experimental process, the sensors were also cleaned as described in subsection 3.2.2, with ultrasonication at intensity 2. They were then immediately placed in the Qsense flow modules after being taken out of the nitric acid bath and flushed with a continuous flow of water. After calibrating the frequencies of the substrates the measurement was started. The method described in section 3.2 was then executed by pumping the solutions to flow across the sensor. Ethanol of concentration (99.5% or 95%) was pumped through the flow module at 200μl/min, before changing to the MPTMS solution to functionalise the surface for 30min at 200μl/min. After functionalisation, ethanol with the same concentration was pumped again at 200μl/min, before changing to water at the same rate. Then the seed solution was run through the modules at 25μl/min for 40min after which the water baseline was pumped again. Then the growth solution was pumped through the module at 25μl/min for 2 hours for the flow measurements or stopped for the stagnant measurement after flushing the module with at least 10 times the 40μl internal volume

above the sensor. After the growth had proceeded for 2 hours, water was again pumped through the system, until a stable frequency level was observed. The substrates were then dried using N_2 for further analysis with SEM.

4

Results and Discussion

The following sections present both the results achieved in this thesis and a discussion of the findings. Starting with discussing the gold nanoparticle seed synthesis and the method of functionalisation. Then the results gained from gold nanorod growth are demonstrated and finally, the real-time measurements taken *in situ* are presented.

4.1 Gold seed synthesis and immobilisation

4.1.1 Electrostatic deposition

Initial experiments in this thesis synthesised and attached larger gold seed particles with a citrate stabilisation. These particles were tested to evaluate the possibility of electrostatically immobilising seeds on a silicon wafer surface. By functionalising the substrate surface with (3-aminopropyl)-triethoxysilane (APTES), positive charges could be created for the negatively charged citrate seeds to bind to, shown in Figure 4.1. As the SiO_2-surface has a negative surface charge the seeds would only attach to the functionalisation, while being repelled by the substrate and each other, creating a homogeneous surface coverage.

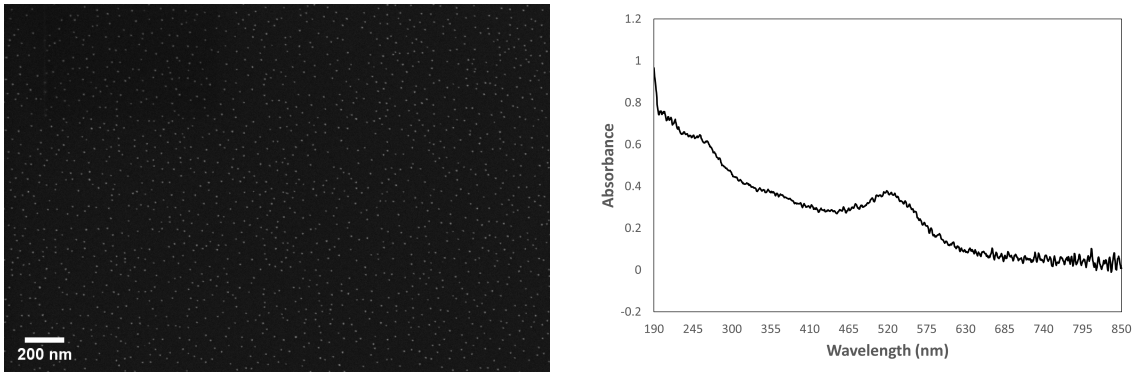

Figure 4.1: On the left is an SEM image at 100k magnification of electrostatically immobilised citrate seed particles on a silicon wafer, and on the right is a UV-vis absorption spectra of the citrate seeds in solution

When the substrate, with its gold seed particles attached in this way, was added to the growth solution, the electrostatic binding was screened by the ions contained in the growth solution. Seeds were then released from the surface and nanoparticle

growth could be seen to occur in the solution as it shifted from clear to purple colour. Thus it was not possible to show conclusively that the rods grew while attached to the surface. As the purpose of the thesis was to demonstrate the possibility to grow nanorods directly on a surface, this method was not investigated further.

4.1.2 Gold seed functionalisation with MPTMS

Fresh gold nanoparticle seeds with CTAB stabilisation were synthesised for each experiment. The gold seeds produced this way were too small for analysis by UV-vis, as the LSPR extinction does not appear in the UV-visible light region for particles of this size, as the dielectric function of particles of this size is not the same, changing their optical properties[11]. The seed formation was determined by the colour of the solution as the Au(III) ions were reduced to metallic gold, which turned light brown as described in the method proposed by L. Scarabelli *et al.*[9]. The solution should therefore have contained seeds with a diameter of ~2-4nm, as the characteristic absorption band at 507nm would be visible once the particles reach an average size of >3.5nm, as can be seen for the citrate seeds in Figure 4.1[9]. Particles at this size are beyond the resolution limit of the Leo Ultra 55 SEM, so a size distribution of the produced seed solutions used in this thesis can not be presented. There are however particles within some of the produced solutions that do appear in the SEM after being chemisorbed to a MPTMS functionalised silicon wafer. These particles can be seen in Figure 4.2, where some particles are as large as ~9nm in diameter.

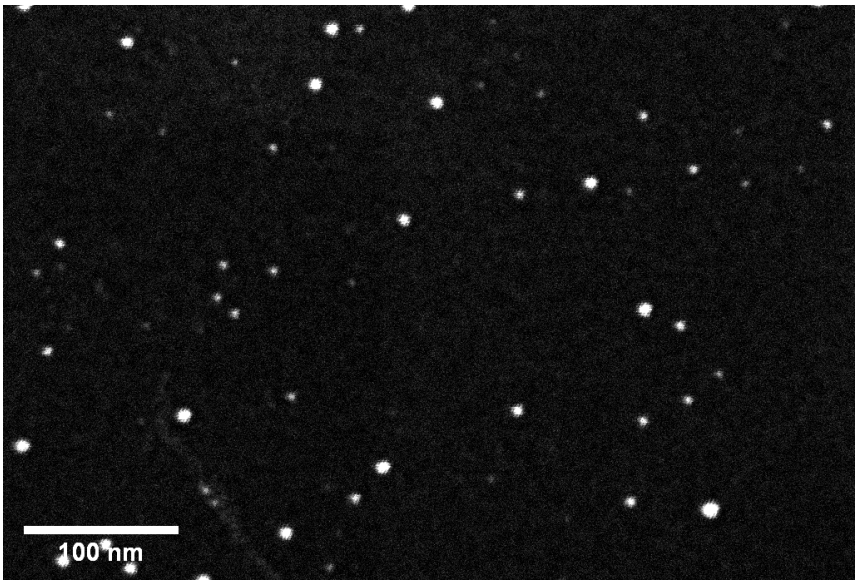

Figure 4.2: SEM image with 500k magnification of a silicon wafer functionalised with MPTMS and CTAB stabilised gold seed nanoparticles

It is however unlikely that seeds of this size made out a large fraction of the seeds that were produced, since the total optical effect of the solution is not coloured by LSPR. The solution may however not be monodisperse for each synthesis, as indicated by varying particle sizes in Figure 4.2. This could be due to several factors. Examples include contamination, poor mixing during nucleation into particles,

creating a wider size distribution of particles, or since particles of this size are not stable for longer periods of time, they may start aggregating or absorbing each other before attaching to the surface. If the functionalisation creates a perfect SAM, the particles may even attach close enough for Ostwald ripening to occur before SEM analysis. However, since the seeds were produced and attached within 30 minutes of analysis, the risk of aggregation should be minimised. The inclusion of these larger sizes in the growth phase of the experiments may however have had an effect on the final particle size distributions and perhaps even the morphologies and therefore the rod yield seen after particle growth.

The substrate cleaning process, where they were immersed in concentrated nitric acid was essential to achieve the rod yield seen in this thesis. The addition of nitric acid etching prevented a wider range of morphologies to grow from the seeds, vastly improving the rod yield. This may be due to a more pristine substrate oxide layer as the acid effectively reduces contaminating sodium, calcium and aluminium atoms on the glass surface[33].

4.2 Gold nanorod formation and dimensions

The gold nanorods that were successfully grown, with a demonstrated high shape yield of ~69% using the method formulated in this thesis, are presented in this section. The aspect ratio (AR) of the nanorods have been shown to be tunable, with the highest and lowest AR achieved presented below in Figure 4.3, along with histograms illustrating the AR-distribution of the synthesis.

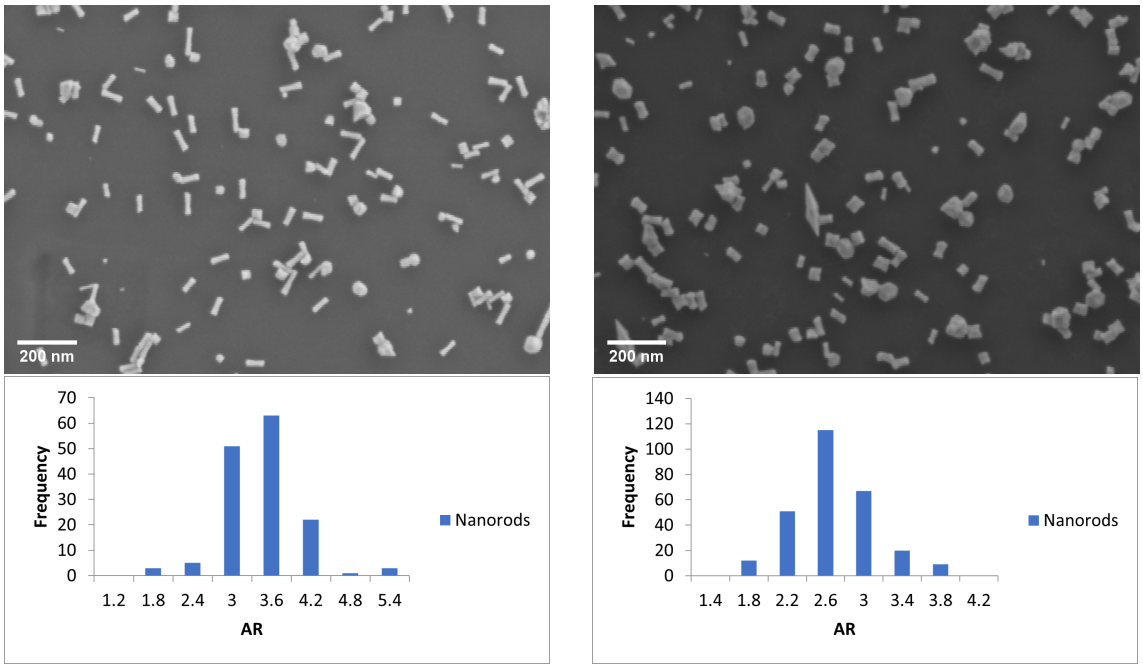

Figure 4.3: SEM images, with 150k magnification, accompanied by histograms showing the AR distribution, of gold nanorods produced by 2 hours growth using recipes containing, $\frac{[AgNO_3]}{[Ascorbicacid]} = {}^{20mM}/_{70mM}$, to the left and ${}^{11mM}/_{90mM}$, to the right

The effect of the gold nanorod growth on the particles' LSPR can be seen evolving over time in the *in situ* UV-Vis spectra in Figure 4.4. Comparing these plots highlight how susceptible seed mediated growth is to contaminations. The measurements were taken in parallel, functionalised in the same MPTMS solution, and were placed in the same seed solution for immobilisation. However, as they were placed into the cuvets, the substrate represented on the right in Figure 4.4 was scratched. This caused seeds to be released from the substrate surface into the growth solution, visibly changing the colour of the solution and contaminating the results.

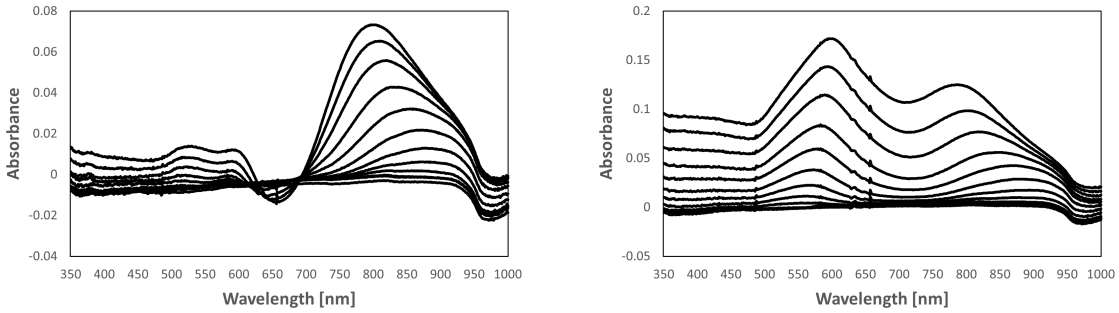

Figure 4.4: *In situ* UV-vis spectras of gold nanorods as they were produced simultaneously by growth recipe $^{14mM}/_{70mM}$ over 2 hours. The right image shows the effect of scratching the surface just before growth. Each increment in absorption represents 10 minutes growth

The experiments included a nucleation control during nanoparticle growth. These substrates were functionalised with MPTMS, but were never placed into the gold seed solution for chemisorption. Figure 4.5 shows the resulting SEM image of one of the glass substrate controls. There the nucleation of gold particles can be seen, which has grown into various morphologies. These particles appeared to nucleate directly on the MPTMS thiol group, as nucleation and the subsequent growth within the solution was not observed through UV-vis analysis. As the spontaneous nucleation of gold on MPTMS did not result in nanorod growth, this mechanism negatively affects the rod yield of the experiments. There also appears to be some deposited gold in the background, but this could be artefacts from the SEM analysis. A potential solution for future studies could be to include an extra step between seed immobilisation and growth, where the substrates could be placed in a solution containing a substance to passivate any remaining free thiol groups left on the surface. This may increase the overall rod yield of the method.

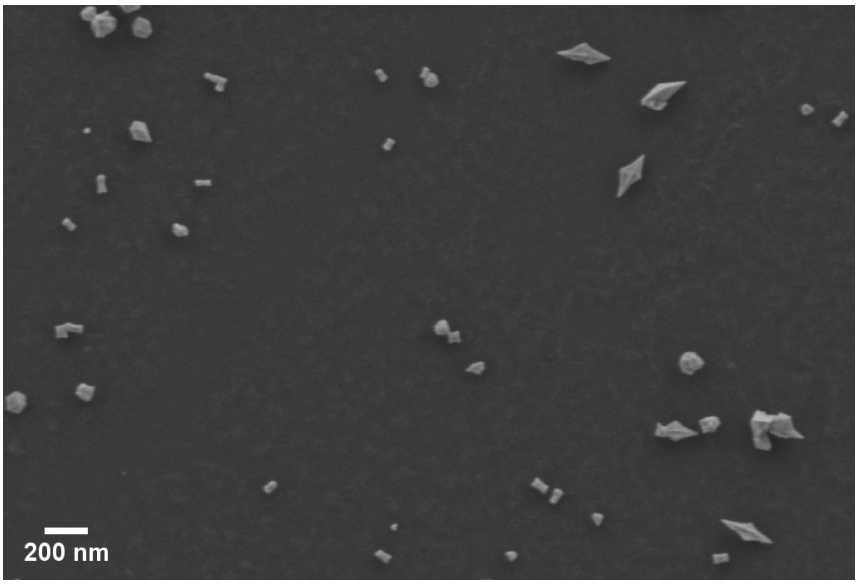

Figure 4.5: SEM image at 70k magnification of a SiO_2 glass control substrate, containing gold nanoparticles that spontaneously nucleated on MPTMS

4.2.1 Impact of silver ions on rod-formation and aspect ratio

The effects of altering the silver ion concentration on the AR and yield of the nanorods was studied as a method of tuning the frequency of LSPR to 800nm. The results from these experiments are presented and discussed in this section and the chosen recipes can be seen in Table 4.1.

Table 4.1: Table presenting the rod yield and average surface coverage of grown particles along with the particle dimensions of each growth solution recipe. C_{AA} and C_{Ag^+} represents the concentrations of ascorbic acid and $AgNO_3$, respectively

Growth recipe C_{Ag^+}/C_{AA}	Rod yield	Surface coverage	Length [nm]	Width [nm]	Aspect ratio
$^{20mM}/_{70mM}$	69.30%	14.80%	65.43 ± 8.28	21.13 ± 3.02	3.16 ± 0.41
$^{14mM}/_{70mM}$	65.79%	6.13%	76.29 ± 12.80	26.23 ± 4.22	2.92 ± 0.31
$^{13mM}/_{70mM}$	54.74%	10.43%	67.57 ± 10.83	23.05 ± 3.63	2.96 ± 0.38
$^{12mM}/_{80mM}$	52.97%	10.07%	69.41 ± 9.18	27.55 ± 4.15	2.56 ± 0.32
$^{11mM}/_{90mM}$	69.00%	16.13%	66.94 ± 9.64	27.64 ± 4.59	2.47 ± 0.33
$^{10mM}/_{100mM}$	68.18%	26.95%	78.62 ± 11.60	39.35 ± 6.69	2.05 ± 0.29

The concentrations of silver nitrate seen in Table 4.1 range from the lowest, 10mM, which was the same as in the original recipe, up to a 100% increase as the highest tested concentration[9]. The surface coverage and rod yield varies, without any observed correlation to the concentrations and the discrepancy can be assumed to be caused by handling errors during or between earlier stages in the synthesis. Examples of such errors could include MPTMS polymerisation during functionalisation due to water contamination or contact with air after seed immobilisation, which could dry or otherwise destabilise the CTAB bilayer causing other morphologies to

grow.

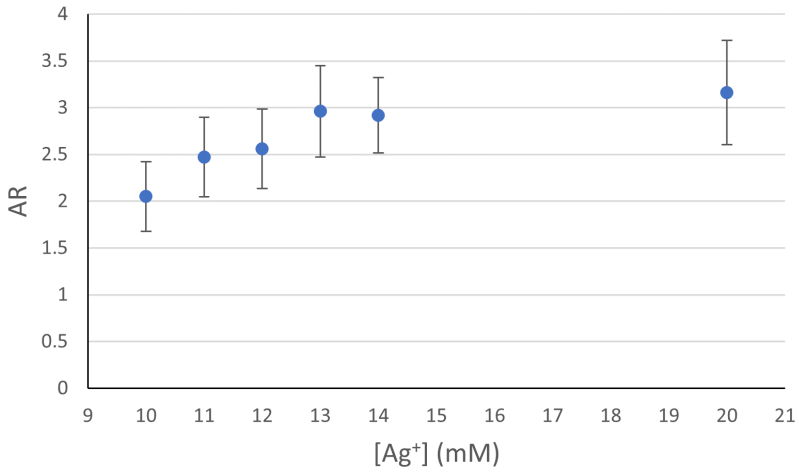

Figure 4.6: Aspect ratio of nanorods grown *in situ* on glass as a function of the concentration of $AgNO_3$. The error bars represent the standard deviation from the average AR

The aspect ratio for the recipes were plotted in Figure 4.6, compared to the concentration of $AgNO_3$ in the growth solution. The recipe ${}^{14mM}/_{70mM}$ produced the rods seen in Figure 4.7, with an AR of 2.92 which had a longitudional LSPR wavelength at the goal wavelength of 800nm, as seen in the UV-vis measurement, similar to the rods produced in solution in the literature using the original recipe, ${}^{10mM}/_{100mM}$[9]. This discrepancy between concentrations and the resulting rod dimensions and LSPR frequency may have been caused by several factors. An example of which could be the particles' decreased degrees of freedom from being bonded to the MPTMS. A large part of the difference between solution-growth and surface-growth of rods could be due to the effects of surface charge on the ion concentrations in the solution. The resulting concentration gradient that occurs in the diffuse layer of charged ions probably had a significant impact on nanorod growth.

The seed mediated growth method is easily disrupted by contaminants and highly affected by factors including changes in reactant concentrations. To increase the AR of gold nanorods, the literature suggests slightly changing several factors, instead of heavily altering one too much which could be detrimental to the yield. These include increasing [$AgNO_3$] and lowering [ascorbic acid] which was done in this thesis[11]. The glass surface is negatively charged and the metal ions that were added to the solution were, Ag^+, Au^+ that were produced by the reduction of Au(III) with ascorbic acid[9]. Therefore, the ${}^{14mM}/_{70mM}$-recipe may have resulted in a similar concentration close to the surface, as ${}^{10mM}/_{100mM}$ may have during growth in solution[34]. Following this instruction however, lowering the concentration of ascorbic acid, could potentially leave some unreacted Au(III) in the solution. These ions could then displace the ions with less charge close to the surface, lowering the Ag/Au-ratio during growth. This can not be confirmed with the analysis performed

in this thesis, but a future study could investigate this effect by including an X-ray photoelectron spectroscopy (XPS) analysis, to measure the elemental composition of the surface-grown particles. This could then be used to find the final Ag/Au-ratio within the *in situ* grown nanorods and compare this to rods grown in solution, to study the effect of the Debye length on growth[34].

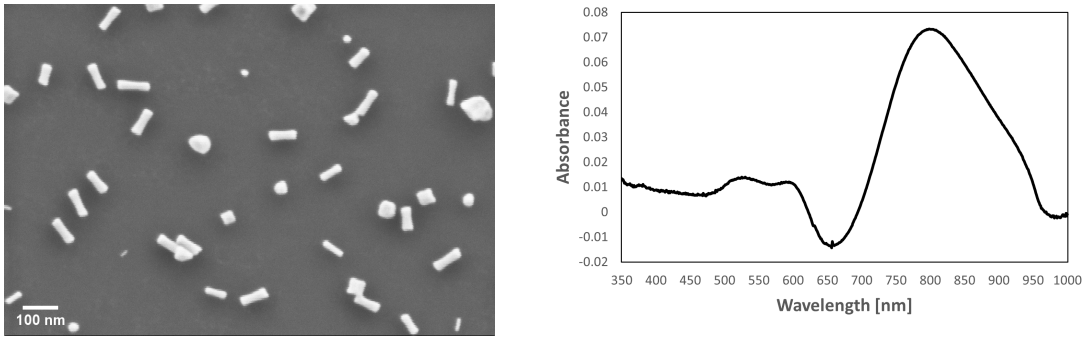

Figure 4.7: SEM image and UV-vis spectra of gold nanorods, taken with 200k magnification, after 2 hours growth using growth recipe $^{14mM}/_{70mM}$, with a longitudinal peak at 799nm

In Figure 4.7, an additional small absorption peak can be seen at ~520nm, next to the transversal nanorod absorption, as well as a widening in the base of the longitudinal peak. These effects are made from the other morphologies seen in Figure 4.7 and by plasmon coupling, which widen the longitudinal band when nanorods are close together, as they are when bound to the surface. The total absorption of the particles had a high peak at 800nm relative to the transversal peak, indicating a high yield of rods with a larger aspect ratio and the right size, summing up to the goal LSPR frequency of this thesis, within the so-called biological window which could be of use for medical device surfaces.

The software imageJ allowed for accurate and quick pixel by pixel analysis of the SEM images. However, the software had difficulty distinguishing particles that appeared too close together and instead merged several particles as one misshapen particle, resulting in a lower rod yield than expected. These particles needed to be manually counted by removing bordering pixels to correct the rod yield, but these particles' dimensions would then remain shortened while measuring the particle AR. To manage this, the rods that had to be sliced by more than a pixel (1-3nm) could not contribute to the dimension averages. This issue did not affect coverage data, as this compares the ratio of light and dark pixels in the image and could be analysed before counting.

4.3 *In situ* analysis

In this section the real-time analysis results conducted *in situ* is presented, showing the particle's evolution over time. First the data gained from QCM-D is presented, separated into each step of the synthesis method, followed by UV-vis data gathered

continuously during growth.

QCM-D analysis was performed to monitor particle growth in real-time in growth solution recipe $^{13mM}/_{70mM}$. The particles grew both in stagnant solution, similar to the procedure outside the QCM-D, and with 25μl flow with fresh growth solution, to compare the effect. QCM-D frequency measurements and SEM images of both can be seen in Figure 4.8.

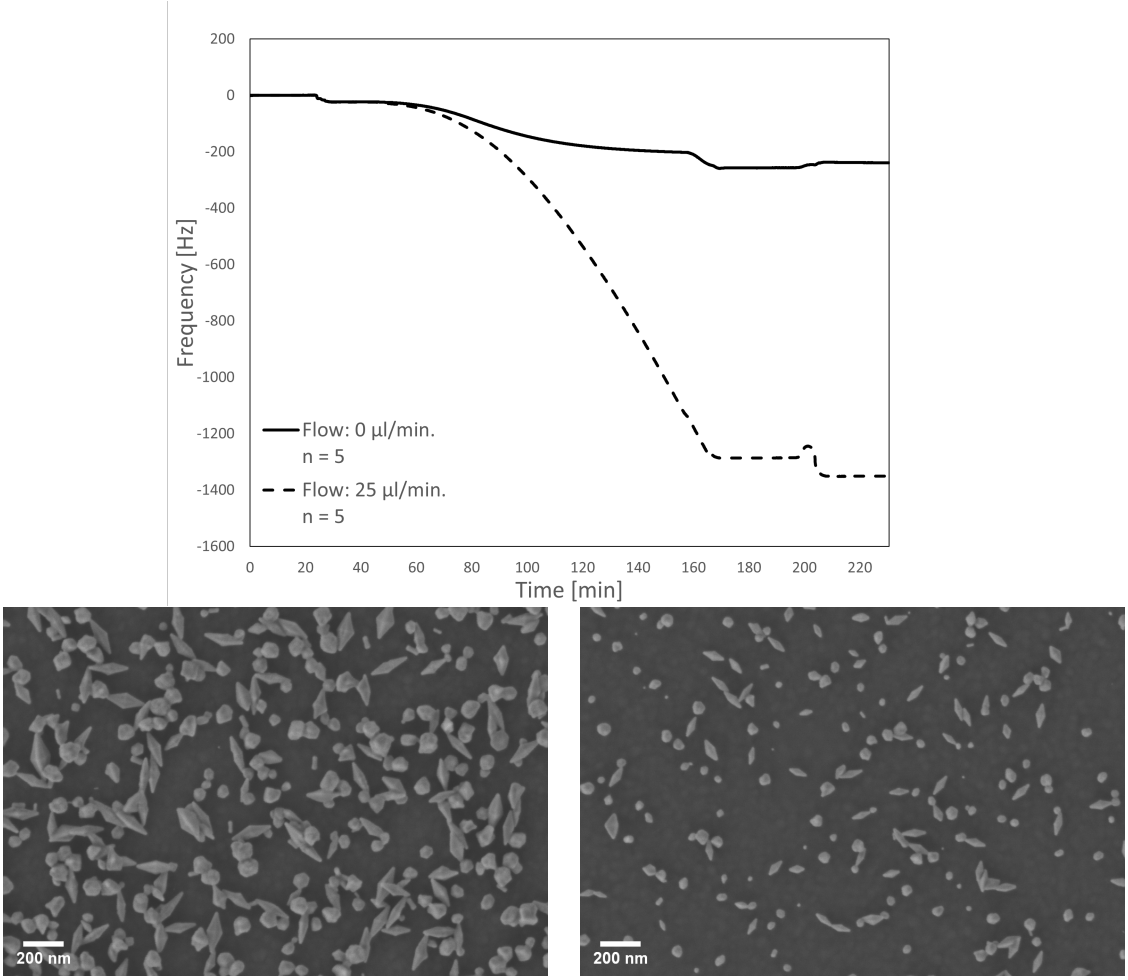

Figure 4.8: QCM-D measurement and 100kx magnified SEM images of the QSX 303 SiO_2 sensors, containing the gold nanoparticles produced during QCM-D after 2 hours of particle growth. The particles in the SEM image on the left grew during flow and on the right in stagnant solution

This QCM-D analysis used sensors treated before the analysis identically outside the QCM-D flow cells, using the same seed functionalisation. The results demonstrate a large increase in growth rate for the sensor which had a continuous flow of fresh growth solution across the surface. This can be seen in the QCM-D data by the second-degree change in frequency over time, while showing no greater effect on the morphologies, creating a few rods during flow, and barely any without flow. Interestingly the density of particles was increased as well. This could indicate nucleation on unoccupied MPTMS thiol sites, where the flow forces the ions in the solution to

reach down closer to the surface. There could also have been varying success during functionalisation, due to contamination.

QCM-D was also used to measure the full method. One such run can be seen in Figure 4.9, where the functionalisation used ethanol (95%) as a solvent to promote hydrolysis. This run is divided into inlets of each synthesis stage, 1. functionalisation, 2. gold seed chemisorption, and 3. particle growth, to be analysed separately.

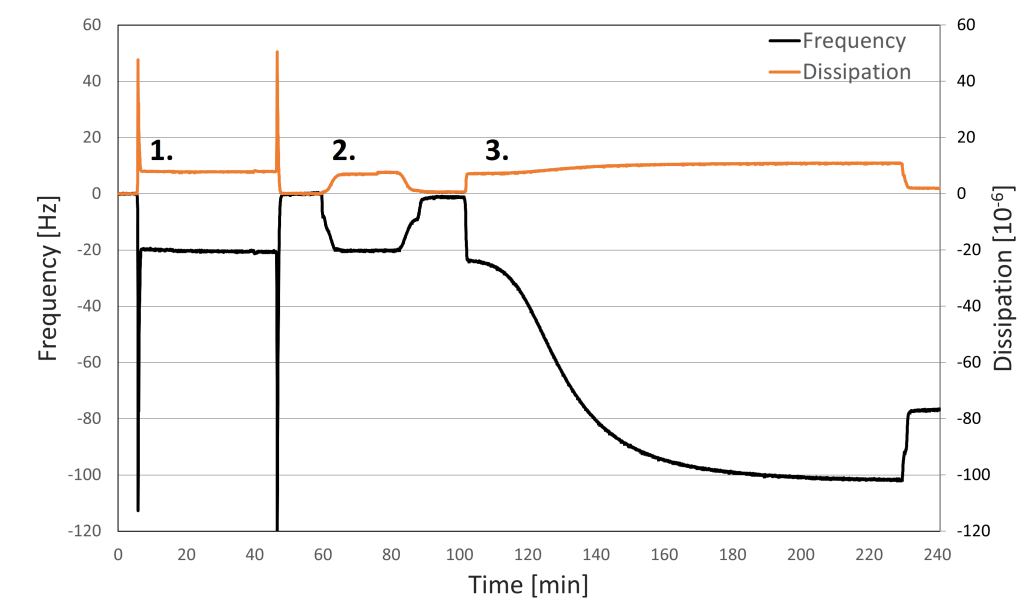

Figure 4.9: QCM-D measurement of the full method using growth recipe $^{14mM}/_{70mM}$ and 2 hours growth on a QSX 303 SiO_2 sensor with no flow. The lines depict an average of the 5th, 7th and 9th overtones, where the black line shows the change in frequency and the orange line represents the energy dissipation rate

4.3.1 Functionalisation

The formation of the SAM of MPTMS can be seen *in situ* in the QCM-D data presented in Figure 4.10, where a lower concentration of ethanol (95%) was used as solvent for the MPTMS during functionalisation, to promote hydrolysis. The QCM-D inlett starts at the baseline with no frequency shift at 0 minutes elapsed time with the substrate mounted in a flow cell filled with a 200μl/min flow of MilliQ water. After 6 minutes, ethanol (95%) is pumped through the cell at the same rate, to remove water before adding MPTMS and to establish a stable measurement after the solvent change causes a frequency spike in the data, with the alcohol solvent before functionalisation. The MPTMS solution is then pumped through the flow cell at 200μl/min flow from 15 minutes into the run to 40 minutes in, where no more change was observed in the frequency. At 40 minutes the visible change in frequency is due to the solvent being changed back to ethanol (95%), before again being exchanged at 47 minutes back to the baseline of pure water.

The frequency measured in pure water before and after functionalisation shifts by

~−0.75Hz for the 9th overtone, over 30 minutes during the 200μl/min flow of fresh MPTMS solution across the substrate. This corresponds to a mass change of ~Δm = 1.475ng/cm^2 over the ~0.1963cm^2 sensing area of the substrate.

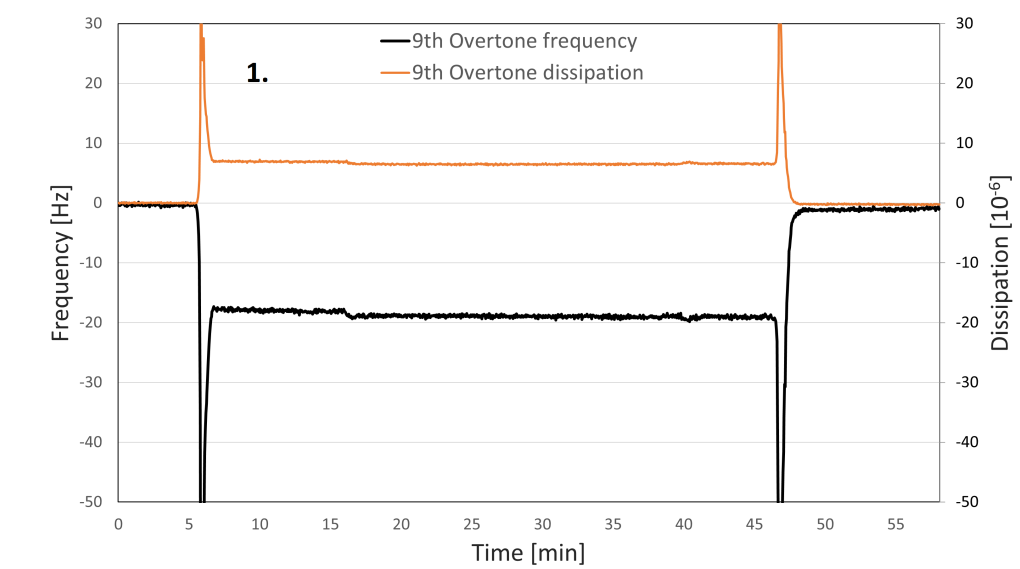

Figure 4.10: QCM-D inlett focusing on the functionalisation of a QSX 303 SiO_2 sensor from Biolin. The MPTMS solution flowed at 200μl/min across the surface

Assuming a homogeneous SAM packing density, this mass on the substrate would correspond to $n \approx 0.045$ MPTMS molecules/nm^2 and thus 1 MPTMS molecule/22nm^2, with potential for the same number of gold seeds to attach to the same area. This fits well with the spherical particle monolayer seen in Figure 4.12. The detected mass was the wet mass of MPTMS, including the influence of molecular interactions with water, so deviations between the number of particles and the number of MPTMS sites were expected. An additional analytical method such as surface plasmon resonance (SPR) would need to be run as well, to gain the dry mass.

4.3.2 Seed immobilisation

After some attempts at functionalising the substrates in QCM-D after excessive rinsing with ethanol (99,5%), the purity of ethanol used for functionalisation was changed to (95%). This was done as it was assumed that the MPTMS solution at this point did not contain enough water close to the surface for the hydrolysis reaction which binds the MPTMS to the SiO_2 surface. The seed immobilisation performed after this functionalisation in the same QCM-D analysis can be seen occurring in Figure 4.11, which starts and ends with ~5 minutes in pure water as a baseline to measure the total mass gained. At 20 minutes and again at 27 minutes the change in frequency is reduced, which could be due to seeds being rinsed off of the sensor without new particles taking their place. As the rate of dissipation seen in orange is shifted more greatly from 0 during the same period, this could be an indication of a build up of particles attaching to, and then being released from a greater distance to the sensor, affecting the hydrodynamic resistance of the substrate.

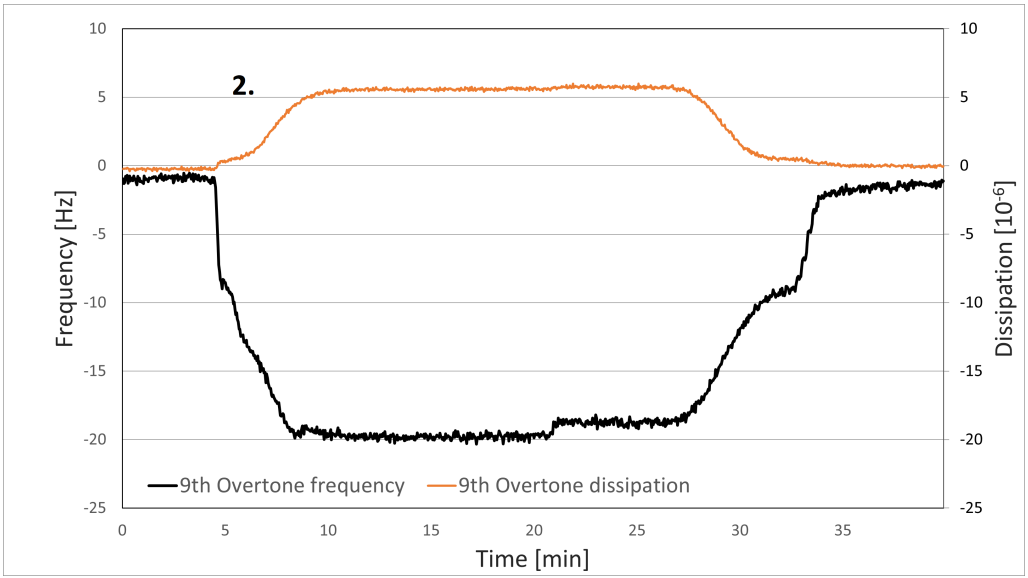

Figure 4.11: Inlett of a QCM-D measurement, focusing on the seed immobilisation on an MPTMS functionalised QSX 303 SiO_2 sensor from Biolin. The seed particles were immobilised while flowing across the surface at 25μl/min

Calculations and image analysis were performed, presented in Appendix A.1, for the seed immobilisation to see if the number of adsorbed seeds remained constant during growth. This was done to help determine the stability of the particles, and to show whether the mechanism driving the particle growth was by mainly absorbing and reducing ions from the solution. An alternative growth mechanism during rod formation could potentially be found through changes in the surface coverage as seeds merge during growth, or as new particles nucleate on the surface. This would not be seen in the QCM-D, as the merging of particles would not affect the mass adsorbed to the surface and nucleation of new particles would be indistinguishable from the absorption of ions. However, running the same calculation with an assumed average seed size of 4nm in diameter instead of the assumed 2nm in Appendix A.1, the results change from 26.8% of particles remaining after growth, to 214.4%. Thus an accurate size determination of the seeds would be required to determine if new particles nucleate during growth, as observed in Figure 4.5 on unoccupied MPTMS molecules, or if seeds merge while growing when they are this close together in a SAM.

4.3.3 Growth

The QCM-D was then finally used to measure the growth of the particles as well, flushing the QCM-D module with growth solution recipe $^{14mM}/_{70mM}$ for 10 minutes before stopping the pump to allow the particles to grow in a stagnant solution for 2 hours, similar to the experimental conditions outside the QCM-D. The resulting QCM-D plot is presented in Figure 4.12, along with an SEM image of the SAM of gold nanoparticles.

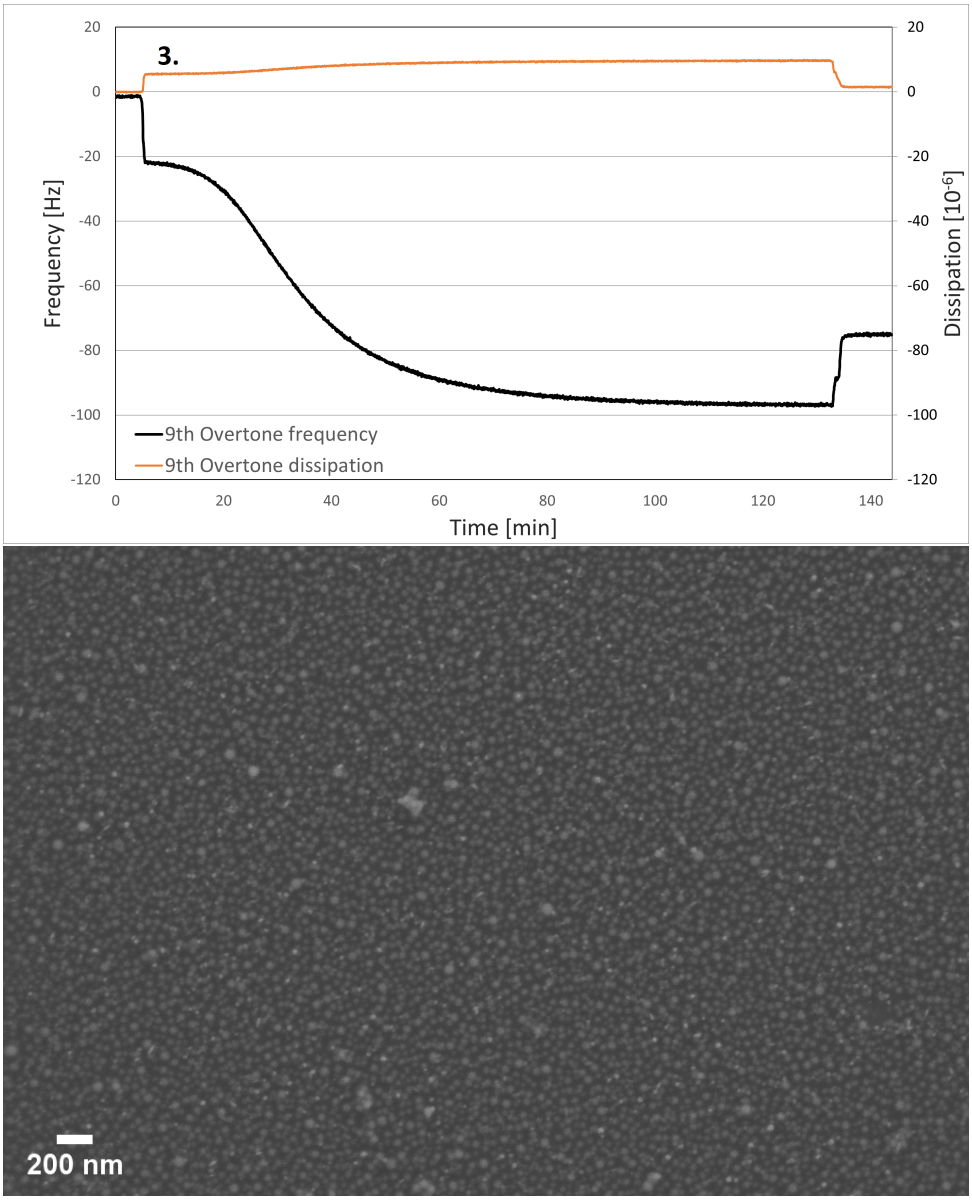

Figure 4.12: Inlett of a QCM-D measurement focusing on the nanoparticle growth in stagnant solution and an SEM image at 50k magnification of the QSX 303 SiO_2 sensor, containing the gold nanoparticles produced after 2 hours growth

The particles in this QCM-D run were chemisorbed with a high density, appearing to not leave much room to grow. The growth may then be restricted in certain directions, which may not align with the capped facets directing the growth. If the particles grow and become close-packed, there may also be a possibility for CTAB to form additional layers across the surface, potentially halting growth in this area. This could perhaps be the reason for the almost stagnating growth rate at the end, as there should have been an abundance of Au^+ ions left in the solution. The frequency change seen in Figure 4.12 corresponded to a reduction of less than 1% of the mass of Au(III) available within the QCM-D module volume of 40μl growth solution to metallic gold on the surface.

5

Conclusion

A method has been formulated for the synthesis and growth of Gold nanorods *in situ* on glass surfaces, demonstrating the possibility to grow and control the morphology of gold nanoparticles even while adhered to a surface. In this method, CTAB stabilised gold nanoseeds are chemisorbed to silica surfaces, using an MPTMS linking molecule. The seeds are then grown into gold nanorods *in situ*, by placing the substrates in a modified growth solution based on a synthesis method for solution-grown gold nanorods. The aspect ratio could be tuned for the surface grown particles by varying the concentrations of $AgNO_3$ and Ascorbic acid in the growth solution. The final aspect ratio however, tends to be lower for rods grown *in situ* when compared to rods grown in solution, so several parameters were tweaked at once. By doing this, the LSPR of the rods was successfully tuned to resonate with and absorb NIR light with a wavelength of 800nm, within the so called biological window. Producing a high yield of gold nanorods with a wavelength of LSPR at 800nm was a goal of this thesis, demonstrating the viability of this method for the potential application as impland device surface material to treat and prevent biomaterials-associated infections.

The shape-yield of the produced nanorods was demonstrated up to 69.3% with a surface coverage of up to 26.95%, which could possibly be increased further in future experiments if needed. The presented rods produced LSPR while irradiated and by 800nm NIR light, the method can be applied in future studies creating surfaces that can potentially prevent and treat implant related infections. The tunable rod-dimensions could make the formulated method useful for other applications as well, where gold nanorods would be required to be attached to substrate surfaces which rods that are pre-grown in solution prove difficult to bind to.

The possibility to use the developed method in surface sensitive analysis techniques was demonstrated as well, which could perhaps be used to further the study of the unclear mechanisms involved in anisotropic gold nanoparticle growth. This was demonstrated by using the same method, with only minor alterations to study the effects of flow. The method produced anisotropic particles, but with a low yield of nanorods. As such, the QCM-D method needs some further development and more QCM-D runs are needed to sort out any remaining handling errors. However, with the QCM-D data that was gained, the method demonstrates the promise of surface sensitive techniques for *in situ* analysis. It also produced data for such things as finding out the correct amount of time each part of the synthesis requires.

5.1 Future work

There are several topics that still need to be studied in future work. First, an analytical method such as X-ray photoelectron spectroscopy (XPS) or nanoscale secondary ion mass spectrometry (nanoSIMS) could be used on the *in situ*-grown gold nanorods, to study the effect of surface charge on growth and ion concentrations. This could be used to compare the $\frac{Ag}{Au}$ ratio in the rods to rods grown to the same LSPR, in solution, investigating the effect of the Debye length, which may cause the ion concentrations of the growth solutions to end up the same close to the metallic surface of the particles. The method should be attempted on other material surfaces as well, adapting the linking molecule to some thiolated molecule suitable for that material, as replicating the growth on other materials would validate the method further, especially if done on common implant device materials. Using materials of varying surface charge could also be of use in the investigation of ionic concentrations during growth.

Cell biology studies on bacterial elimination using LSPR generated heat would be good to include in future studies, to demonstrate the applicability of this method. Future work in this area could also include adapting the seed immobilisation by screening the ionic strength during chemisorption, to change the density of particles. By using a flow cell this could potentially be used to create a substrate with a coverage gradient of gold nanorods across the surface, which in turn would be useful to find the optimal coverage for photothermal eradication of bacteria using LSPR. Another way to potentially affect coverage and perhaps increase rod yield, could be to study the nucleation of new gold particles on free MPTMS thiol groups, as shown to occur in the control seen in Figure 4.5. These sites may be the cause of other morphologies and they could potentially be passivated in a future study the see the effect on rod yield. The thiols may also be good candidates to develop a seedless method for *in situ* nanorod growth, as it can be done in solution[35]. This may be a better way to utilise the SAM of thiols, and could potentially increase both rod yield and particle density.

Working with QCM-D for *in situ* analysis of an adapted version of this thesis' formulated synthesis method, gave indications of areas which could be investigated further in future work. Examples include, the occurance of MPTMS polymerisation seen as clusters of particles, or additional CTAB bilayer formation. Potentially obscuring a layer of particles the SEM struggles to distinguish and capping their growth. This background pattern was previously assumed to be artifacts or aberrations of using SEM analysis on glass, warranting further investigation into the existence of these particles, and if they do exist, what stopped their growth. The experiments made it possible to see how the growth rate develops over time, highlighting the mass transport limitation on particle size and coverage. More experiments need to be performed in a future study focused on these findings to confirm or deny these hypotheses, and to answer how the use of flow to transport ions to the particles impact the final morphology, as well as whether the depletion of the concentration of gold or silver ions in the growth solution is necessary for high yield rod growth.

Bibliography

[1] Rabih O Darouiche. Treatment of infections associated with surgical implants. *New England Journal of Medicine*, 350(14):1422–1429, 2004.

[2] JW Costerton, L Montanaro, and Carla Renata Arciola. Biofilm in implant infections: its production and regulation. *The International journal of artificial organs*, 28(11):1062–1068, 2005.

[3] WJ Metsemakers, R Kuehl, TF Moriarty, RG Richards, MHJ Verhofstad, O Borens, S Kates, and M Morgenstern. Infection after fracture fixation: current surgical and microbiological concepts. *Injury*, 49(3):511–522, 2018.

[4] Maria Pihl, Ellen Bruzell, and Martin Andersson. Bacterial biofilm elimination using gold nanorod localised surface plasmon resonance generated heat. *Materials Science and Engineering: C*, 80:54–58, 2017.

[5] Andrew M Smith, Michael C Mancini, and Shuming Nie. Second window for in vivo imaging. *Nature nanotechnology*, 4(11):710–711, 2009.

[6] K Lance Kelly, Eduardo Coronado, Lin Lin Zhao, and George C Schatz. The optical properties of metal nanoparticles: the influence of size, shape, and dielectric environment, 2003.

[7] Archana N. Rao, Mahender N. Avula, and David W. Grainger. Chapter 11 - aging and the host response to implanted biomaterials. In Stephen F. Badylak, editor, *Host Response to Biomaterials*, pages 269–313. Academic Press, Oxford, 2015. ISBN 978-0-12-800196-7. doi: https://doi.org/10.1016/B978-0-12-800196-7.00011-6. URL `https://www.sciencedirect.com/science/article/pii/B9780128001967000116`.

[8] Kaixi Bi, Yiqin Chen, Qiang Wan, Tuo Ye, Quan Xiang, Mengjie Zheng, Xuejiao Wang, Qing Liu, Guanhua Zhang, Yongtao Li, et al. Direct electron-beam patterning of transferrable plasmonic gold nanoparticles using a haucl 4/pvp composite resist. *Nanoscale*, 11(3):1245–1252, 2019.

[9] Leonardo Scarabelli, Ana Sánchez-Iglesias, Jorge Pérez-Juste, and Luis M Liz-Marzán. A "tips and tricks" practical guide to the synthesis of gold nanorods, 2015.

[10] Vivek Sharma, Kyoungweon Park, and Mohan Srinivasarao. Shape separation of gold nanorods using centrifugation. *Proceedings of the National Academy*

of Sciences, 106(13):4981–4985, 2009. doi: 10.1073/pnas.0800599106. URL https://www.pnas.org/doi/abs/10.1073/pnas.0800599106.

[11] Jorge Pérez-Juste, Isabel Pastoriza-Santos, Luis M Liz-Marzán, and Paul Mulvaney. Gold nanorods: synthesis, characterization and applications. *Coordination chemistry reviews*, 249(17-18):1870–1901, 2005.

[12] Xiaohua Huang, Svetlana Neretina, and Mostafa A El-Sayed. Gold nanorods: from synthesis and properties to biological and biomedical applications. *Advanced materials*, 21(48):4880–4910, 2009.

[13] Alaaldin M Alkilany and Catherine J Murphy. Toxicity and cellular uptake of gold nanoparticles: what we have learned so far? *Journal of nanoparticle research*, 12(7):2313–2333, 2010.

[14] Ellen E Connor, Judith Mwamuka, Anand Gole, Catherine J Murphy, and Michael D Wyatt. Gold nanoparticles are taken up by human cells but do not cause acute cytotoxicity. *Small*, 1(3):325–327, 2005.

[15] Yi Zou, Yanxia Zhang, Qian Yu, and Hong Chen. Photothermal bactericidal surfaces: killing bacteria using light instead of biocides. *Biomaterials Science*, 9(1):10–22, 2021.

[16] Andrei S. Dukhin and Philip J. Goetz. Chapter 2 - fundamentals of interface and colloid science. In Andrei S. Dukhin and Philip J. Goetz, editors, *Characterization of Liquids, Dispersions, Emulsions, and Porous Materials Using Ultrasound (Third Edition)*, pages 19–83. Elsevier, third edition edition, 2017. ISBN 978-0-444-63908-0. doi: https://doi.org/10.1016/B978-0-444-63908-0.00002-8. URL https://www.sciencedirect.com/science/article/pii/B9780444639080000028.

[17] Alex Langford, Michael Bruchsaler, and Manish Gupta. Suspension properties and characterization of aluminum-adjuvanted vaccines. In *Practical Aspects of Vaccine Development*, pages 225–266. Elsevier, 2022.

[18] Jonathan Moore and Eleonora Cerasoli. Particle light scattering methods and applications. 2017.

[19] Hyunho Kang, Joseph T Buchman, Rebeca S Rodriguez, Hattie L Ring, Jiayi He, Kyle C Bantz, and Christy L Haynes. Stabilization of silver and gold nanoparticles: preservation and improvement of plasmonic functionalities. *Chemical reviews*, 119(1):664–699, 2018.

[20] María Victoria Lozano, Manuel J Santander-Ortega, and María José Alonso. In vitro relevant information for the assessment of nanoparticles for oral drug administration. *Nanotechnology for oral drug delivery*, pages 419–458, 2020.

[21] Neyvis Almora-Barrios, Gerard Novell-Leruth, Peter Whiting, Luis M Liz-Marzan, and Nuria Lopez. Theoretical description of the role of halides, silver, and surfactants on the structure of gold nanorods. *Nano letters*, 14(2):871–875, 2014.

[22] Rahul Kumar, Leonardo Binetti, T Hien Nguyen, Lourdes SM Alwis, Arti Agrawal, Tong Sun, and Kenneth TV Grattan. Determination of the aspect-ratio distribution of gold nanorods in a colloidal solution using uv-visible absorption spectroscopy. *Scientific reports*, 9(1):1–10, 2019.

[23] Jing Cheng, Lan Ge, Bin Xiong, and Yan He. Investigation of ph effect on gold nanorod synthesis. *Journal of the Chinese Chemical Society*, 58(6):822–827, 2011.

[24] Michelle L Personick, Mark R Langille, Jian Zhang, and Chad A Mirkin. Shape control of gold nanoparticles by silver underpotential deposition. *Nano letters*, 11(8):3394–3398, 2011.

[25] Jose A da Silva, Paulo A Netz, and Mario R Meneghetti. Growth mechanism of gold nanorods: the effect of tip–surface curvature as revealed by molecular dynamics simulations. *Langmuir*, 36(1):257–263, 2019.

[26] Nadine Harris, Martin G. Blaber, and George C. Schatz. *Optical Properties of Metal Nanoparticles*, pages 1950–1969. Springer Netherlands, Dordrecht, 2012. ISBN 978-90-481-9751-4. doi: 10.1007/978-90-481-9751-4_22. URL `https://doi.org/10.1007/978-90-481-9751-4_22`.

[27] Bhavya Sharma, Renee R. Frontiera, Anne-Isabelle Henry, Emilie Ringe, and Richard P. Van Duyne. Sers: Materials, applications, and the future. *Materials Today*, 15(1):16–25, 2012. ISSN 1369-7021. doi: https://doi.org/10.1016/S1369-7021(12)70017-2. URL `https://www.sciencedirect.com/science/article/pii/S1369702112700172`.

[28] Jan Mistrik, Safa Kasap, Harry E Ruda, Cyril Koughia, and Jai Singh. Optical properties of electronic materials: fundamentals and characterization. In *Springer handbook of electronic and photonic materials*, pages 47–82. Springer, 2017.

[29] Richard Gans. Über die form ultramikroskopischer goldteilchen. *Annalen der Physik*, 342(5):881–900, 1912.

[30] B Indumathy, R Gunasekhar, P Sathiyanathan, and Anand Prabu Arun. Chemistry and applications of organosilanes–an overview. *ECS Transactions*, 107(1): 14539, 2022.

[31] Ray F Egerton. The scanning electron microscope. In *Physical principles of electron microscopy*, pages 125–153. Springer, 2005.

[32] Ralf Richter, Keith Rodenhausen, Nico Eisele, and Mathias Schubert. *Coupling Spectroscopic Ellipsometry and Quartz Crystal Microbalance to Study Organic Films at the Solid–Liquid Interface*, pages 391–417. 05 2018. ISBN 978-3-319-75894-7. doi: 10.1007/978-3-319-75895-4_17.

[33] HK Jang, YD Chung, SW Whangbo, TG Kim, CN Whang, SJ Lee, and S Lee. Effects of chemical etching with nitric acid on glass surfaces. *Journal of Vacuum Science & Technology A: Vacuum, Surfaces, and Films*, 19(1):267–274, 2001.

[34] Yan Zeng, Stefan Grandner, Cristiano LP Oliveira, Andreas F Thünemann, Oskar Paris, Jan S Pedersen, Sabine HL Klapp, and Regine von Klitzing. Effect of particle size and debye length on order parameters of colloidal silica suspensions under confinement. *Soft Matter*, 7(22):10899–10909, 2011.

[35] Kang Liu, Yanru Bu, Yuanhui Zheng, Xuchuan Jiang, Aibing Yu, and Huanting Wang. Seedless synthesis of monodispersed gold nanorods with remarkably high yield: synergistic effect of template modification and growth kinetics regulation. *Chemistry–A European Journal*, 23(14):3291–3299, 2017.

A
Appendix

A.1 Analysis for QCM-D seed adsorption

This appendix details the image analysis and calculations made to compare the data from the gold seed immobilisation performed in the QCM-D, to the SEM image of the final, grown particles. In Figure A.1 the part of the QCM-D run focusing on the chemisorption of gold seeds can be seen, along with a SEM image taken of the QSX 303 SiO_2 sensor after the particles had grown for 2 hours and the QCM-D measurement was finished. The growth was performed in a stagnant growth solution, to mimic the conditions in the method for rod growth outside the QCM-D.

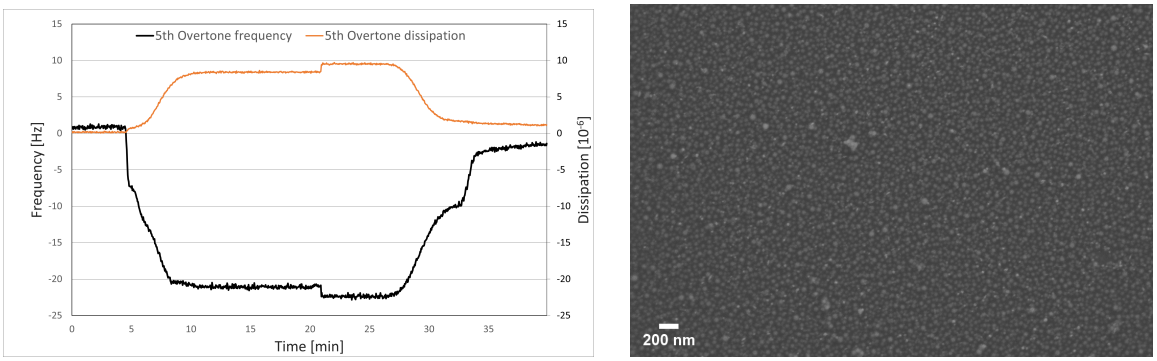

Figure A.1: Inlett of a QCM-D measurement focusing on the 5th overtone frequency change during seed immobilisation and an SEM image of the sensor after 2 hours growth, containing the gold nanoparticles produced during QCM-D by growth recipe ${}^{14mM}/_{70mM}$. The particles in the image on the right grew in stagnant solution

First the frequency change detected by the QCM-D was used to calculate the mass of the adsorbed seeds, using Equation 2.10,

$$\Delta m = -C\frac{\Delta f}{n} = -17.7\frac{-2.5}{5} = 8.85\frac{ng}{cm^2}$$

since $A_{sensing} \approx 0.19634854cm^2$ for the 5th overtone and below, the mass adsorbed to the sensor surface was, $m_{seeds} \approx 1.7377ng$. It was assumed that all adsorbed seeds were spheres of pure gold with a diameter of $2nm$. Gold has a density of $\rho_{Au} = 19.320 \cdot 10^{-12}\frac{ng}{nm^3}$, so the number of seeds attached to the sensor could be determined to $n_{seeds} = 21\,472\,243\,696$, a seed density of $\delta_{\text{QCM-D}} \approx 109\,357\,239\,624.48\frac{seeds}{cm^2}$.

This was then compared to the number of particles seen in the SEM image, taken after the QCM-D measurement, seen in Figure A.1. The number of particles $n_{particles} = 5745$ was determined using the software ImageJ. The number gained was lower than the actual amount of seeds, since multiple seeds were often counted as one, which could not be separated manually since there were too many particles like this in the image. The density of particles was then calculated by,

$$\delta_{\text{SEM}} = \frac{n_{particles}}{A} = \frac{5745}{5389.47nm \cdot 3636.84nm} = 293.103 \cdot 10^8 \frac{particles}{cm^2}$$

where A was the area of the SEM image.

$$\frac{\delta_{\text{SEM}}}{\delta_{\text{QCM-D}}} \approx 26.8\%$$

Comparing the densities of particles in the SEM image and gained from the QCM-D data, with an assumed seed size of 2nm, ~26.8% of the particles remain.

DEPARTMENT OF CHEMISTRY AND CHEMICAL ENGINEERING
CHALMERS UNIVERSITY OF TECHNOLOGY
Gothenburg, Sweden
www.chalmers.se

CHALMERS
UNIVERSITY OF TECHNOLOGY